

MIT Open Access Articles

Chemical vapour deposition

The MIT Faculty has made this article openly available. **Please share** how this access benefits you. Your story matters.

Citation: Nature Reviews Methods Primers. 2021 Jan 14;1(1):5

As Published: <https://doi.org/10.1038/s43586-020-00005-y>

Publisher: Nature Publishing Group UK

Persistent URL: <https://hdl.handle.net/1721.1/131818>

Version: Author's final manuscript: final author's manuscript post peer review, without publisher's formatting or copy editing

Terms of use: Creative Commons Attribution-Noncommercial-Share Alike



Chemical Vapour Deposition

Luzhao Sun^{1,2}, Guowen Yuan³, Libo Gao^{3†}, Jieun Yang⁴, Manish Chhowalla^{4†}, Meysam Heydari
Gharahcheshmeh⁵, Karen K. Gleason^{5†}, Yong Seok Choi^{6,7}, Byung Hee Hong^{6,7†} and Zhongfan
Liu^{1,2†}

[†] Correspondence should be addressed to Z.F.L. (zfliu@pku.edu.cn), L.B.G. (lbhao@nju.edu.cn),
M.C. (mc209@cam.ac.uk), K.K.G. (kkgleasn@mit.edu), and B.H.H. (byunghee@snu.ac.kr).

¹ *Center for Nanochemistry, Beijing Science and Engineering Center for Nanocarbons, Beijing
National Laboratory for Molecular Sciences, College of Chemistry and Molecular Engineering,
Peking University, Beijing 100871, P. R. China.*

² *Beijing Graphene Institute, Beijing 100095, P. R. China.*

³ *National Laboratory of Solid State Microstructures, School of Physics, Collaborative Innovation
Center of Advanced Microstructures, Nanjing University, Nanjing 210093, China.*

⁴ *Department of Materials Science and Metallurgy, University of Cambridge, Cambridge, UK.*

⁵ *Department of Chemical Engineering, Massachusetts Institute of Technology, Cambridge, MA,
USA.*

⁶ *Graphene Research Center, Advanced Institute of Convergence Technology, Suwon 16229,
Korea & Department of Chemistry, Seoul National University, Seoul 08826, Korea.*

⁷ *Graphene Square Inc., Suwon 16229, Korea.*

21 Abstract

22 Chemical vapour deposition (CVD) is a powerful technology for producing high-quality solid
23 thin films and coatings. While widely used in modern industries, it is continuously being
24 developed as it is adapted to new materials. Today, CVD synthesis is being pushed to new
25 heights with the precise manufacturing of both inorganic thin films of two-dimensional (2D)
26 materials and high-purity polymeric thin films that can be conformally deposited on various
27 substrates. In this Primer, an overview of the CVD technique including instrument construction,
28 process control, material characterization, and reproducibility issues is provided. By taking
29 graphene, 2D transition metal dichalcogenides (TMDs) and polymeric thin films as typical
30 examples, the best practices for experimentation involving substrate pre-treatment, high-
31 temperature growth and post-growth processes are presented. Recent advances and scaling-up
32 challenges are also highlighted. By analyzing current limitations and optimizations, we also
33 provide insight into possible future directions for the method, including reactor design for high-
34 throughput and low-temperature growth of thin films.

[H1] Introduction

Chemical vapour deposition (CVD) is a widely used materials-processing technology where thin films are formed on a heated substrate via a chemical reaction of gas-phase precursors. In contrast to physical vapour deposition methods, such as evaporation and sputtering, CVD offers a clear advantage by relying on chemical reactions that enable tunable deposition rates as well as high quality products with excellent conformality. The greater demand for semiconductor thin films starting after World War II was the initial driving force for rapid development of CVD technology¹⁻⁵. Recently, low-dimensional materials such as carbon nanotubes, graphene, and two-dimensional (2D) transition metal dichalcogenides (TMDs) have injected new vitality into the electronics industry⁶⁻⁸ and introduced more stringent requirements for successful CVD of these materials with high purity and fine structure. CVD allows the tuning of the structures and properties of the resulting products⁹, and a variety of advanced CVD systems and their variants have been developed, such as plasma-enhanced CVD (PECVD)² and metal organic CVD (MOCVD)⁴ (BOX 1). Usually, CVD does not require high vacuum working environments, making it a popular technology for electronics, optoelectronics, surface modification, and biomedical applications.

Irrespective of the variations in CVD types, the fundamental process is similar and consists of the following common elementary steps^{10,11} (**Fig. 1**). First, the reactant gases are transported into the reactor. These reactant gases then either react with each other in the gas phase to form intermediate reactants and gaseous by-products via homogeneous reactions, or diffuse

57 directly through the boundary layer to the substrate. In both cases, the reactant gases and the
58 intermediate reactants adsorb onto the heated substrate surface and diffuse on the surface.
59 The subsequent heterogeneous reactions at the gas-solid interface lead to continuous thin film
60 formation via nucleation, growth, and coalescence as well as formation of reaction byproducts.
61 Finally, any gaseous products and unreacted species desorb from the surface and are carried
62 away from the reaction zone. The gas-phase reactions occur when the temperature is
63 sufficiently high or additional energy is introduced, for example, in the form of plasma. In
64 addition, the heterogeneous reaction is essential if the deposition reaction relies on the surface
65 catalysis of the underlying substrate, such as in the case of the catalytic growth of graphene on
66 metal surface.

67

68 In this Primer, we first provide an overview of the CVD instrumentation setup before
69 describing best practices for material preparation and characterization using the growth of
70 graphene on metal and dielectric substrates as representative examples of catalytic CVD and
71 non-catalytic CVD processes, respectively. We then demonstrate the flexibility of this method
72 by discussing important applications of CVD, including growth of binary and ternary 2D
73 materials and polymeric thin films. We also highlight recent progress and challenges when
74 scaling-up this technology, an important aspect of CVD when applied to industry. Finally, we
75 discuss what affects experimental reproducibility, current limitations of the technique, and
76 future developments of CVD together with exploration of new materials.

77

[H1] Experimentation

To obtain high-quality thin films by CVD, suitable equipment is needed, and custom-built systems provides the flexibility of operation often desired by CVD researchers. In this section, we will discuss a series of designs that satisfy the requirements of materials synthesis, including the heating methods, gas-flow control, the loading of substrate, etc. In addition, the growth parameters, including substrate, temperature, atmosphere, pressure etc. are essential for controlling the quality of as-grown materials as well as the reaction rate (growth rate). Here, we will introduce CVD growth of graphene following the procedure of substrate pretreatment, heating, annealing, high-temperature growth and cooling.

[H2] CVD equipment

A CVD system must meet the following basic requirements: delivery of the gas-phase reactants in a controllable manner; provision of a sealed reaction chamber; evacuation of the gases and control of the reaction pressure; supply of the energy source for the chemical reactions; treatment of the exhaust gases to obtain safe and harmless levels; and automatic process control to improve the stability of the deposition process. **Fig. 2** shows a typical CVD system consisting of a gas delivery system, reaction chamber, vacuum system, energy system, exhaust gas treatment system, and automatic control system.

[H3] Gas delivery system

Safety and process control are two of the key aspects of this design, especially considering the possibility of using high-pressure, toxic, flammable and explosive gas, liquid or solid precursors.

The gaseous reactants are usually stored in high-pressure gas bottles placed in cool places outdoors or in cabinets at a constant negative pressure, to ensure safety. The gas supply line starts at the outlets of the high-pressure gas bottles, which are fitted with mechanical pressure regulators to control the pressure, and ends at the inlet of the reaction chamber. Valves (for

102 example, ball shut off, needle shut off and pneumatic valves) and metal gasket seal connectors
103 are often used to ensure a good sealing performance.

104 Mass flow controllers are essential for the gas supply, where the gas flow rate is automatically
105 set via feedback control according to the mass of flowing gas. Liquid source reactants are
106 delivered by “bubbling” a carrier gas controlled by the mass flow controller (**Fig. 2b**)^{12,13}. Solid
107 source precursors that are less volatile are introduced to the reaction chamber by dissolution in
108 a suitable solvent¹⁴ or by sublimation into the gas-phase¹⁵⁻²¹.

109 [H3] Reaction chamber

110 The horizontal (**Fig. 2a**)²²⁻²⁴ and vertical (**Fig. 2c-e**)^{25,26} configurations are the two main
111 configurations of the reaction chamber (**Box 1**). The reaction chamber itself is usually quartz
112 tube, widely employed in semiconductor manufacturing because of its tolerance to high
113 temperatures and to rapid heating and cooling. A gas inlet injector is connected to the chamber
114 using a metal flange, which is fitted with cooling components. To guarantee the gas flow is
115 laminar, a gas distributor with through-holes is usually employed (**Fig. 2c-e**)^{22,25}. The substrate is
116 usually located on a substrate holder (also known as a “boat” or “susceptor”) composed of
117 quartz or graphite because of their good chemical stability and high-temperature
118 resistance^{22,27,28}. In order to meet the target deposition characteristics (thickness, composition,
119 etc.), the configuration of the substrate holder and the deposition conditions (total gas flow, gas
120 composition, temperature, pressure, etc.) must be optimized via experimental and numerical
121 process engineering studies^{22,25,26,29,30}. In manufacturing applications, a cooling chamber with a
122 loading/unloading subsystem is necessary to improve the productivity.

123 [H3] Vacuum system

124 Purging the deposition chamber to start the deposition process and obtaining the necessary
125 pressure for transport of the reactants relies on the vacuum system, where measurement and
126 control of the vacuum are essential and complement one another. To measure the pressure of
127 the vacuum system, various gauges are alternated: the Bourdon gauge, piezo sensor,
128 capacitance manometer, and diaphragm manometer are the main mechanical gauges, which
129 can measure the vacuum by detecting physical changes in the strain or electrical capacitance,
130 for example. The Bourdon gauge is inexpensive and has a long life, but it does not have an
131 electronic output, and so is not suitable for feedback control (**Fig. 2f**). Using a capacitance
132 manometer, a measurement range of four orders of magnitude can be achieved for almost any
133 gas, and the signal can be transported to an electronic display or a feedback controller (**Fig. 2g**).
134 The diaphragm manometer operates the same way as the capacitance manometer, only with a
135 smaller range of measurement. In addition, gas property gauges, such as thermocouple gauges
136 and the Pirani gauge, are inherently inaccurate, since their value is determined by the types of
137 gases and temperatures; however, when calibrated, they can be used to measure certain
138 conditions. Furthermore, ionization gauges are commonly employed under high or ultra-high
139 vacuum conditions.

140 To control the pressure, the use of a throttle valve or a needle valve is effective, and the
141 downstream flow rate can be controlled by adjusting the opening degree of the valve gate³¹.
142 The chamber pressure will then stabilize when the flow rate of the incoming gas is equal to that

143 of the exhaust, which can be automatically or manually controlled by real-time pressure
144 monitoring³¹.

145 Pumps provide the driving force for the vacuum and mass-transport within the system. For a
146 CVD system, mechanical pumps are adequate for many operations, and can provide a vacuum
147 of 1 Pa. Oil pumps are cheaper than dry pumps of the same power, but bring additional
148 contaminants into the system. If the reaction chamber is large, a rotary pump (pumping speed
149 ranging from 0.5 - 325 L s⁻¹) with a Roots pump (50 - 35,000 L s⁻¹) is a good choice for fast
150 exhaust. Finally, a vacuum isolation valve (also known as a block valve) is used between the
151 outlet of the CVD chamber and the pump to shut off the pumping process.

152 [H3] Energy system.

153 For a thermal CVD process, the heating components, thermal insulation structure, and
154 temperature measuring elements are important. **Fig. 2a** shows a common resistance heating
155 furnace, which consists of three heating zones and aluminum silicate insulating cotton to
156 ensure a uniform temperature field over a sufficient length. Thermocouples, which are the
157 most common temperature measuring device, are placed between the quartz tube and the
158 heating components, and are connected to a proportional–integral–derivative (PID) regulator.
159 Several types of thermocouples exist (including B, K, R and S), which are suitable for application
160 under different conditions³². In the case of a large reactor (diameter >25 cm), the inclusion of
161 thermocouples inside the chamber is necessary to calibrate the temperature. Cold-wall reactors
162 most frequently use a graphite heater that introduces an electrical current into the
163 chamber^{29,33}, and a pyrometer is commonly employed to measure the temperature. Plasma can

164 also be used to provide energy by electrical discharge of the gaseous media; in this case, the
165 electron temperatures are significantly higher than the neutral and ion temperatures^{34,35}. As an
166 example, an inductively-coupled plasma source is illustrated in **Fig. 2a**, and this can be placed
167 against part of the reaction chamber for facile integration into the tube reactor. The geometry
168 and materials of the substrate holder also influence the heat transfer, while radiant heating
169 with a halide lamp³⁶, electric induction³⁷, or laser can be used to specifically heat the substrate.

170 [H3] Exhaust gas treatment system

171 The by-products and unreacted chemical substances of CVD tend to be flammable, toxic or
172 harmful to the pumps, and therefore must be safely treated. This is usually done with either
173 one or a combination of components such as cold traps, chemical traps, particle traps, wet
174 scrubbers and vents^{14,18}. A cold trap is used to condense volatile gases and cool exhaust gases
175 to stop the temperature of the vacuum pump oil from increasing. In addition, various corrosive
176 gases can be reacted or adsorbed by passing through a chemical trap, and a particle trap can
177 provide protection against pump wear. To further convert the exhaust into harmless substances,
178 a burning component or a wet scrubber can also be employed³².

179

180

181 [H2] Experimental methods for materials growth

182 Here, we introduce the material preparation process by using graphene as an example (**Fig. 3**).
183 Graphene is a nanomaterial consisting of single layer sp^2 bonded carbon atoms that is
184 challenging to synthesize in a controllable manner because the growth of high-quality

185 monolayer graphene films requires a catalytic metal substrate, although thicker graphene can
186 be grown on a non-catalytic insulating substrate as long as a higher temperature or additional
187 energy supply is available to promote decomposition of the precursors.

188 [H3] Substrate pre-treatment

189 Selecting an appropriate substrate is essential for CVD growth because different substrate
190 catalytic abilities and carbon solubilities result in different graphene growth modes. Transition
191 metals (for example, copper and nickel)^{38,39} and insulating substrates (for example, SiO₂, Al₂O₃,
192 and glass)⁴⁰⁻⁴² are typical substrates on which the heterogeneous catalytic reaction and the gas-
193 phase reaction dominate the growth processes, respectively. To grow high-quality graphene,
194 cleaning of the substrate is necessary. Electrochemical polishing, for example on copper foil,
195 can be employed to reduce the level of contaminants and decrease the surface roughness (**Fig.**
196 **3a**). As for silicon wafers or sapphire wafers, typical cleaning procedures employed in the
197 semiconductor community (such as picking) are applicable (**Fig. 3e**).

198 [H3] Heating and annealing

199 After loading the substrate onto the substrate holder and transporting it to the desired location
200 in the CVD chamber, the gate is closed and the chamber is checked for any air leakage. The
201 substrate is then heated to 1000 °C and annealed under a non-reactive atmosphere (**Fig. 3b**).
202 During this procedure, the introduction of very small quantities of oxygen into the chamber can
203 aid in reducing the nucleation density of graphene by burning any carbon-containing
204 contaminants^{43,44} that could seed graphene during the growth process. Hydrogen is commonly
205 introduced to reduce and activate the weakly oxidized copper surface. In addition, a

206 temperature gradient is beneficial for preparing a single crystal metal substrate to promote
207 subsequent graphene growth (**Fig. 3b**)^{28,45-47}.

208 [H3] High-temperature growth

209 Graphene growth is initiated by introducing a hydrocarbon precursor (methane is most
210 commonly used) that decomposes into active carbon species to fuel growth of graphene. If the
211 substrate is a metal with a relatively high catalytic ability and a low carbon solubility, such as
212 copper, the hydrocarbon precursors are initially adsorbed onto the substrate prior to step-by-
213 step decomposition into active carbon species under the form of CH_x (x = 3, 2, 1, 0)⁴⁸.

214 Subsequent growth takes place through nucleation, growth and coalescence of the graphene
215 seeds to produce a continuous film (**Fig. 3c**)^{49,50}. During the nucleation stage, the nucleation
216 density and orientation of the nuclei determining the domain size of the graphene film are
217 influenced by temperature, the concentration of active carbon species, the surface properties
218 of substrate, etc. In the surface catalysis-dominated process, the formed graphene islands
219 continuously expand until they merge into a film: this is called the self-limited growth mode.

220 Research on the growth kinetics of this self-limited mode is essential to increase the growth

221 rate and improve the graphene quality. According to the Arrhenius equation $k = Ae^{\frac{-E_a}{RT}}$, the
222 growth rate k is exponential with $-E_a/T$, where E_a is the growth activation energy, T is
223 temperature, and R is the universal gas constant. Various strategies are effective at increasing
224 the growth rate and include introducing surface oxygen, employing metals with high catalytic
225 activity, or increasing the temperature and concentration of the precursors. However, the gas-
226 phase reaction when catalyzed on the surface of the metallic substrate can produce significant

227 amounts of by-products and induce the formation of amorphous carbon contaminants^{20,51},
228 which is often overlooked.

229 For non-metallic substrates (for example, SiO₂ or Al₂O₃), if the precursor concentration and
230 temperature are both sufficiently high, the thermally-decomposed active carbon species can
231 deposit onto the substrate and form a graphene film (**Fig. 3f**)^{30,40,41,52}, where gas-phase
232 decomposition reactions plays a crucial role. In this case, employing high-energy plasma can
233 promote the decomposition of the carbon precursor and lower the growth temperature
234 (<600°C)³⁴. However, due to a lack of catalytic activity from the substrate and a reaction
235 temperature below the graphitization temperature, the quality of the graphene grown using
236 this setup is poor compared to graphene grown on a copper surface^{9,42}.

237 [H3] Cooling

238 The cooling process also contributes to the growth of graphene. If the substrate is a metal with
239 a high carbon solubility, such as nickel, the carbon dissolved in the bulk nickel will segregate
240 and form few-layer graphene sheets^{11,53}. Through designing a synergistic binary alloy (such as
241 Cu/Ni, Ni/Mo, Co/Mo) as a substrate and controlling the cooling rate, the number of graphene
242 layers that form can be controlled during the segregation process (**Fig. 3d**)^{54,55}. The thermal
243 expansion mismatch between graphene and its underlying substrate will also result in wrinkles
244 (standing collapsed structures on the graphene surface) and folds (folded wrinkles or folded
245 graphene) during cooling (**Fig. 3g**)⁵⁶⁻⁵⁹. The carbon solubility⁶⁰ in 1000 °C and thermal
246 expansion⁶¹ of typical substrates are listed in Table 1.

247 Finally, fast cooling, which is achieved by either moving the samples out of the hot zone or by
248 moving the furnace, is commonly employed to increase production efficiency^{9,62}. A
249 programmable cooling procedure can also be used to achieve a desired structure in the
250 produced materials^{62,63}. As a rule of thumb, the flow rates of reactant gases (such as hydrogen
251 and methane) are usually maintained during the cooling process to protect the as-formed
252 graphene film from etching by oxygen leaked from the atmosphere. After the temperature
253 drops below 100 °C, the furnace chamber gate can be opened and the samples can be unloaded
254 from the substrate holder.

255

256 [H1] Results

257

258 CVD is directly related to some of the properties of the as-grown materials. In order to assess
259 the CVD method, the as-grown materials must be characterized in-depth to obtain
260 morphological and structural information. Using the CVD growth of graphene as an example,
261 we describe a number of characterization methods to assess the macroscopic quality, atomic
262 structure, electronic structure, and purity of the resulting graphene (Table 2). A transfer process
263 of the as-grown graphene from the metal catalytic substrate to a target substrate is usually
264 necessary when assessing graphene quality because an appropriate substrate is important for
265 some characterization techniques.

266 [H2] Assessing materials quality and structure

267 Optical microscopy^{9, 68} is a simple and quick tool to identify the macroscopic morphology of
268 graphene. Its lower resolution yields information such as the location of graphene on the

269 substrate, the number of graphene layers and their shape, etc. Optical microscopy is widely
270 used for exfoliated graphene on SiO₂/Si, but is only effective on some silicon substrates with a
271 specific oxide thickness such as 90 nm and 280 nm⁶⁴. For CVD-grown graphene on metal
272 substrates such as copper, nickel, platinum, ruthenium, etc., the graphene usually first needs
273 to be transferred onto these SiO₂/Si substrates for optical microscopy observation (**Fig. 4a**)⁶⁵⁻⁶⁸.
274 However, for the case of graphene grown on copper, selectively oxidizing the graphene/copper
275 interface can cause the oxidized copper to act as a specific substrate⁶⁹⁻⁷¹ and reveal the
276 graphene individual domain [G] shapes, surface coverage, layer numbers or grain boundaries.
277 Graphene domains are delineated by grain boundaries, thus increasing the crystal size of the
278 substrate as well as bonding uniformly-oriented grains seamlessly will help minimize the
279 concentration of grain boundaries. In addition, the multi-function optical microscopy modes of
280 dark-field or polarized light can also increase the image contrast⁷².

281 Scanning electron microscopy (SEM) is another popular tool to characterize the morphology of
282 graphene, as it provides nanoscale spatial resolution and greater depth of field than optical
283 microscopy. It utilizes the attenuation effect of graphene layers on secondary electrons emitted
284 from the underlying substrate^{7,69,73,74}. Normally, in SEM images, a graphene-covered region is
285 darker than the bare substrate (including metal and SiO₂/Si). The color of these regions darkens
286 as the number of graphene layers increases, which is beneficial for distinguishing the layer
287 number of graphene (**Fig. 4b**)^{43,75}. The side-attached Everhart-Thornley detector is the most
288 frequently used, which allows high contrast images at low acceleration voltage ($V_{acc} \leq 5$ kV). The
289 electron energy and density of electron beam should be carefully set according to the

290 conductivity of the substrate because the electron beam will inevitably break atomic lattices in
291 graphene.

292 Atomic force microscopy (AFM) is an important method to measure surface morphology at a
293 subnanometer-scale resolution^{7,39,67}, and its multi-functions can also measure mechanical,
294 electrical and magnetic properties⁷⁶. AFM scans a sharp tip over a sample surface without
295 electron or photon interactions. The surface roughness, thickness, cleanliness, wrinkles, domain
296 sizes and shapes, as well as the bonding status of CVD-grown graphene can all be obtained by
297 this technique (**Fig. 4c-d**)^{51,77-79} for both graphene on its original substrate and graphene
298 transferred on an insulating substrate. Owing to the van der Waals interactions between
299 graphene and the underlying substrate, the thickness of monolayer graphene is usually
300 between 0.6 nm and 1.5 nm, which is much larger than graphene's interlayer spacing of 0.34
301 nm.

302

303 [H2] Assessing atomic structure

304 CVD-grown graphene can be affected by adsorbed atoms and molecules, and display distorted
305 lattices, grain edges, or grain boundaries, so it is important to analyze its atomic structure.
306 Similar in operation to AFM, scanning tunneling microscopy (STM) is another proximal probe
307 imaging technology based on the quantum tunneling effect. It has very high spatial resolution
308 because of the exponential relationship between the tunneling current and the distance
309 between the conducting surface and the sharp scanning tip, which means the honeycomb
310 lattice of graphene or its morphology over hundreds of nanometers with atomic resolution can

311 be easily acquired⁸⁰. Being a surface-sensitive technique, STM characterization requires that the
312 graphene be on a conductive and ultra-smooth substrate. STM images clearly present the point
313 defects, atomic structures of grain boundaries, or the edges of graphene⁸⁰⁻⁸², with zigzag edges
314 preferred in CVD-grown graphene grains on various metals (FIG. 4e)^{80,83-85}. STM also confirms
315 that CVD-grown graphene films retain continuous atomic lattices over metal steps and perfect
316 lateral heterostructure between graphene and hexagonal boron nitride (*hBN*) (FIG. 4f)⁸⁶⁻⁸⁹. The
317 strong coupling between graphene and the growth substrate often gives rise to Moiré patterns
318 (FIG. 4g), and these superstructures vary with their twist angles and the strength of their
319 interactions^{57,90-92}.

320 Transmission electron microscopy (TEM) is a commonly used technique to image the atomic
321 structures of lattices, strains, defects, grain boundaries⁹³⁻⁹⁶ of materials, including graphene and
322 other 2D materials. It has very high resolution, with a recently demonstrated lateral resolution
323 lower than 0.1 nm⁹⁷. Samples for TEM imaging must be suspended or supported on an ultra-
324 thin film, so designed micro-grids with through-holes or a carbon membrane are usually
325 employed. If the TEM is fitted with an aberration corrector, the operation voltage can be
326 reduced and a subnanometer-scale resolution can be achieved. By using an aberration-
327 corrected annular dark-field scanning TEM (ADF-STEM), graphene's grain boundary structures
328 with distorted pentagonal, heptagonal and octagonal rings have been observed (**Fig. 4h**)⁹⁴.

329 In addition to the above techniques, electron backscatter diffraction (EBSD)⁴⁶, X-ray diffraction
330 (XRD)^{98,99}, selected area electron diffraction (SAED)¹⁰⁰ and low energy electron diffraction
331 (LEED)⁹⁶ are also used to characterize CVD-grown graphene. EBSD and XRD are usually used to

332 measure the crystalline orientation of the growth substrate, such as Cu(111), Pt(100), Ru(0001),
333 etc. SAED implemented in a TEM is usually used to confirm the crystalline orientation of
334 graphene, and the SAED pattern can be used to calibrate the lattice constant of graphene. The
335 measurement conditions of LEED requires an ultra-high vacuum and an ultra-smooth surface,
336 and its reduced operation voltage is safer for most 2D materials.

337 [H2] Assessing electronic structure and purity

338 Spectroscopic techniques can provide information regarding the bonding status, electronic
339 structures and purity of CVD graphene through the interactions between atomic lattices and
340 photons with different energies.

341 Graphene was characterized early on using Raman spectroscopy^{101,102}, which relies on **Raman**
342 **scattering [G]** and provides information about lattice vibrations (i.e. phonons) in materials.
343 Similar to exfoliated graphene on SiO₂/Si, the Raman spectrum of CVD-grown graphene mainly
344 consists of four vibration modes¹⁰¹: a layer-dependent C peak (29 – 44 cm⁻¹), a defect-
345 dependent D peak (1340 – 1380 cm⁻¹), a hexagonal lattice-dependent G peak (1550 – 1620 cm⁻¹),
346 and a 2D peak by two phonons process (2650 – 2760 cm⁻¹). All the above values are collected
347 using a laser wavenumber of 532 nm. By fitting the experimental data with a Lorentzian
348 function, the position, shape, full-width-at-half-maximum and relative intensity of the Raman
349 peaks can be obtained, from which information such as the layer number, defects, strain, and
350 doping level of CVD-grown graphene can be extracted (**Fig. 4i-j**)^{66,103,104} for both graphene on
351 metals and graphene transferred on other substrates. As an example, during CVD of graphene
352 on metal, the metal substrate and the high temperature will introduce doping and strain in the
353 graphene: this is easily characterized by the shift and relative intensity ratio of the G peak and

354 2D peak compared to graphene's intrinsic status^{78,90} (i.e. when it is in its suspended exfoliated
355 initial state). In addition, CVD-grown graphene usually has point defects, grain boundaries, or
356 wrinkles, all of which contribute to the D peak^{105,106} (**Fig. 4j**).

357 CVD graphene usually couples with the metal substrates, which alters its electronic structure
358 significantly and causes it to exhibit p-type or n-type doping, an opened bandgap, etc.¹⁰⁷. These
359 effects can be detected by angular resolution photoemission spectroscopy (ARPES)¹⁰⁸ and
360 scanning tunneling spectroscopy (STM)⁹⁰. The Dirac cone of graphene in its intrinsic state is
361 located at the Fermi level, while the position of the Dirac point for CVD graphene on metals
362 usually shifts because of the charge transfer to or from the growth substrates¹⁰⁷⁻¹⁰⁹. For
363 example, the Dirac point for monolayer graphene grown on copper is usually found at -450 – -
364 300 meV with n-type doping and a bandgap of 50 – 350 meV (FIG. 4k)¹¹⁰. In contrast to the
365 large scanning area by angular resolution photoemission spectroscopy, scanning tunneling
366 spectroscopy detects the electronic structure at atomic resolution. Similarly to STM, it requires
367 graphene to have a conductive and smooth substrate, and can measure the doping type,
368 bandgap and the density of states at the atomic scale (**Fig. 4l**)⁹⁰.

369 For heterogeneous doping in CVD-grown graphene, X-ray photoelectron spectroscopy, energy
370 dispersive spectroscopy and electron energy loss spectroscopy (EELS) yield the binding energy,
371 element species and the relative elemental ratio¹¹¹. With energy dispersive spectroscopy or
372 electron energy loss spectroscopy equipped to a TEM, the element distribution can also be
373 imaged at atomic resolution.

374

375

376 [H1] Applications

377 In addition to graphene, 2D materials consisting of two or more elements such as TMDs, *h*BN,
378 Mo₂C, Bi₂O₂Se, etc. and polymeric thin films can also be successfully synthesized by CVD. In
379 contrast to growing graphene, synthesizing TMDs requires more complicated growth
380 parameters because of the solid precursors and phase control needed. Compared to traditional
381 solution-based polymerization, the CVD synthesis of polymeric thin films shows its unique
382 advantages in terms of conformity and high-purity.

383 [H2] CVD for 2D materials growth

384 CVD is the most widely used method for making high quality monolayer TMDs in a laboratory
385 setting¹¹²⁻¹¹⁴. The simplest method is thermal CVD¹¹⁵, where powders of precursors are
386 sublimated at high temperature to form a vapour that condenses as single crystal monolayered
387 TMDs on substrates without substrate-assisted catalysis. Thermal CVD results in deposition of
388 discontinuous triangular crystals along with amorphous and multi-layered products. Despite
389 this, its simplicity and accessibility have made it the most widely studied and utilized method
390 for synthesis of high quality TMDs such as MoS₂, WS₂, WSe₂, MoSe₂ and their
391 heterojunctions¹¹⁶⁻¹¹⁸. In thermal CVD synthesis of TMDs, the reaction chamber (usually a tube
392 furnace as shown in **Fig. 5**) is typically heated to 650 – 900 °C in a nitrogen (N₂) environment. At
393 this high temperature, the precursor powder (such as MoO₃ for MoS₂) is reduced by the sulfur
394 vapour to form volatile suboxides (e.g. MoO_{3-x}). These suboxide compounds then diffuse to the
395 substrate and further react with sulfur vapour to grow MoS₂ films in the form of triangles
396 (shown in the optical microscopy image in **Fig. 5**) that are single layers.

397

398 While uniform and continuous growth of TMDs with thermal CVD is difficult to achieve, some
399 progress has been made on increasing the size of the monolayer crystals by adding salt (NaCl)
400 to the precursors¹¹⁹. The role of salt is not yet clear but it likely facilitates the sublimation of
401 transition metal precursors, even as Na or Cl can be introduced as impurities in the as-grown
402 material. Theoretical work has shown that presence of sodium on the substrate can influence
403 the formation kinetics of MoS₂¹²⁰. The role of sodium on the rapid growth of MoS₂ was verified
404 by producing large-area MoS₂ monolayers on soda-lime glass (composed of SiO₂, Na₂O and
405 CaO)¹²¹. Another challenge in thermal CVD of TMDs is the nucleation of monolayers on
406 technologically relevant substrates that are typically atomically smooth. Graphene-like
407 molecules such as PTAS (perylene-3,4,9,10-tetracarboxylic acid tetrapotassium acid salt) and
408 PTCDA (perylene-3,4,9,10-tetracarboxylic dianhydride) have been used as seed promoters and
409 templated growth of TMDs¹²². In addition, since nucleation of monolayer crystals occurs at
410 atomic edges, substrates such as sapphire with abundant atomic steps have also proved useful
411 in achieving large monolayer crystals¹²³.

412 Recently, significant effort has been devoted to achieving highly uniform wafer scale TMD films
413 using metal-organic CVD (MOCVD)^{122,124}. MOCVD vaporizes metal-organic precursors of both
414 the transition metal and the chalcogen at lower than growth temperatures to achieve uniform
415 monolayer TMDs. For MOCVD growth of wafer-scale MoS₂ and WS₂¹²⁴, molybdenum
416 hexacarbonyl (Mo(CO)₆), tungsten hexacarbonyl (W(CO)₆), and diethyl sulphide ((C₂H₅)₂S) for
417 Mo, W, and S were used as sources. The precursors are directly introduced into a growth
418 furnace heated at 550°C in an H₂ and Ar atmosphere. The key to uniform and continuous
419 monolayers with MOCVD is that the number of nucleation sites is kept low and the lateral

420 growth from those nuclei is allowed to proceed very slowly – it took over 26 hours to fully cover
421 the surface of a 4-inch Si wafer (~10 cm in diameter)¹²⁴. MOCVD also allows precise control of
422 the concentration and supply of the precursors.

423 Similarly to thermal CVD, alkali metal salts also play a crucial but somewhat unclear role in the
424 synthesis of large domains and the suppression of nucleation sites in MOCVD. NaCl can
425 suppress nucleation and achieve monolayer growth of MoS₂^{125, 131}. In NaCl-assisted growth, the
426 salt is typically placed with the substrates in the furnace, which is not a scalable strategy. The
427 average lateral size of MoS₂ in salt-assisted growth was found to be ~60 μm with an electron
428 mobility of 100 cm²V⁻¹s⁻¹ at cryogenic temperatures, indicating the high crystalline quality of the
429 salt-assisted as-grown MoS₂¹²⁶.

430 The most common TMDs synthesized with thermal and MOCVD growth are MoS₂, WS₂, MoSe₂
431 and WSe₂ (Table 3). While significant effort has also been devoted to growing monolayers of
432 metallic TMDs (e.g. NbS₂, TaS₂ and VS₂^{127,128}), these are difficult to grow with CVD because the
433 powder transition metal or metal oxide precursors require very high processing temperatures
434 and equivalent metal organic precursors have yet to be developed. Despite this difficulty, CVD
435 has been used to synthesize forms of niobium disulfide (Nb_{1.35}S₂) that possess very high
436 electrical conductivity¹²⁸. Molten salts can also play a role in reducing the melting points of
437 precursors to form oxychlorides, which in turn can help with increasing the rate of growth of
438 metallic TMDs. In a method for synthesizing metallic TMDs (TiS₂, PtSe₂, PtTe₂, NbS₂, NbSe₂,
439 NbTe₂, VS₂, and VSe₂, etc.) using molten salts¹²⁷, metal oxide precursors like Nb₂O₅ were mixed
440 with NaCl powder and used thermal CVD to grow triangular monolayers.

441 In addition to 2D TMDs, other 2D binary compounds such as *h*BN, Mo₂C and ternary Bi₂O₂Se
442 can also be successfully grown using CVD (Table 3). *h*BN is a 2D insulator with a bandgap of 5.9
443 eV, and plays an important role in advanced electronic devices as a gate dielectric layer or a
444 protecting encapsulator. CVD growth of *h*BN looks very similar to graphene in many aspects
445 (substrate, carrier gas, temperature), except for the solid precursor ammonia borane (NH₃-BH₃),
446 which is the most frequently used^{98,129,130}. 2D Mo₂C, a 2D transition metal carbide, belongs to a
447 family of materials that shows many intriguing properties such as excellent catalytic activity and
448 superconductivity. Large areas of Mo₂C have been grown using methane as a precursor and
449 molybdenum as a substrate, where a copper foil on molybdenum melts during heating and
450 forms an Mo-Cu alloy that serves as diffusion layer for molybdenum atoms and guarantees the
451 chemical reaction leading to the formation of α-Mo₂C crystals¹³¹. Similarly, TaC can also be
452 grown by using tantalum as a substrate¹³². Finally, ternary 2D compounds such as Bi₂O₂Se can
453 also be successfully grown by rationally designing the precursors and the substrate. For
454 example, 2D Bi₂O₂Se is a semiconductor with high carrier mobility, in which the interaction
455 between the charge-carried layers is stronger than the Van der Waals interactions¹³³. Therefore,
456 to therefore achieve atomically thin films and avoid vertical growth, mica and SrTiO₃ have been
457 used as substrates to exploit the stronger interaction^{19,134}.

458 [H2] CVD for growing polymeric thin films

459 Complementing well-established solution-based methods, CVD extends the realm of utility for
460 polymer thin films^{135,136}. CVD is compatible with insoluble macromolecules including many
461 fluoropolymers, electrically conductive polymers and cross-linked organic networks. Its low
462 growth temperatures (typically around 25 °C) and solvent-free nature allow CVD polymers to

463 form directly on fragile substrates including papers, textiles and plant leaves, without a costly or
464 complex transfer step. CVD polymerization even can be accomplished directly onto low-
465 volatility liquid surfaces^{136,137}. CVD polymers can have high purity since the small molecule
466 reactants used are easily purified and there is no possibility of residual solvent in the films¹³⁵.
467 Low defect levels are essential for device applications as well as for surfaces interacting with
468 living cells and tissues¹³⁸, as highlighted below.

469 CVD polymeric layers can conformally follow the geometrical features of the underlying surface,
470 yielding the same film thickness in all locations¹³⁹. Such conformal coverage is essential for
471 coating three-dimensional devices, modifying the internal surfaces of porous materials and
472 membranes, and for maintaining open pores in breathable fabrics and wearable electronics. In
473 contrast, solution coatings are typically non-conformal, as surface tension can blanket the top
474 of a porous surface without coating the interior of the pores. When blanketing closes off pores,
475 surface area is lost for interfacial processes like catalysis and molecular separations. . Shear
476 thinning, capillary forces and meniscus formation present in liquid-based coating processes also
477 cause variations in film thickness over the geometric features in the substrate. The absence of
478 surface tension in CVD processes also avoids pinhole formation by de-wetting even in sub-10
479 nm thick CVD polymer films¹³⁶. Ultrasmooth CVD polymers (< 1 nm root mean square
480 roughness) also reduce pinhole formation produced by excursions in surface roughness which
481 exceed the film thickness.

482 The properties and reactivity of CVD polymers can be tuned and optimized at both the surface
483 and in the bulk via their organic functional groups^{135,136}. To date, dozens of organic functional

484 groups have been incorporated into CVD polymers and include amine, carboxylic acid, epoxy,
485 hydroxyl, perfluorocarbon, and zwitterionic moieties. Many of these organic functional groups
486 permit further surface functionalization of CVD polymers with biomolecules and
487 nanoparticles¹³⁵. High densities of organic functional groups can lead to changes in film
488 thickness and changes in properties in response to external variations such as temperature,
489 humidity, light or pH^{140,141}. Such responsive CVD polymers have been demonstrated for sensing
490 and actuation, smart surfaces, molecular separations and controlled drug release¹⁴²⁻¹⁴⁴.

491 The functional groups of CVD polymers can also be used to control surface energy from
492 superhydrophobic to superhydrophilic. Low surface energy lubricious CVD polymer release
493 layers are used commercially, for example in molds used to manufacture rubber tires and in
494 seals and gaskets used in advanced manufacturing¹⁴⁵. Hydrophobic CVD fluoropolymer
495 conformal nanolayers maintain stamp features fidelity during high speed flexographic
496 printing¹⁴⁶. The precision of surface energy control achieved with conformal CVD polymers has
497 also been exploited in directed self-assembly processes for defining sub-10 nm features and for
498 patterning substrates with 3D topography¹⁴⁷⁻¹⁴⁹.

499 Dielectric CVD polymers are commercially used for protection of electronic and medical
500 devices¹³⁵. CVD organic insulators have also been integrated into lightweight and mechanically
501 flexible devices, including thin film transistors, logic circuits, flash memory and energy
502 harvesting^{136,150}. Conformal hybrid organic/inorganic polymer thin films containing boron or
503 phosphorous have enabled the doping of 3D Fin Field Effect Transistors¹⁵¹.

504 Electrically conducting CVD polymers are attractive as flexible transparent conductors for
505 optoelectronic devices, electrochemical energy storage, and electrocatalysis¹⁵². The
506 conductivity of CVD-grown polymer films can be 6000 S cm^{-1} ¹⁵³, exceeding the values of all
507 previously reported conducting polymer thin films¹⁵⁴ and reaching into the standard range for
508 conductivity of brittle transparent inorganic conductors such indium tin oxide (ITO). In addition,
509 a resurgence of interest in the thermal properties of CVD conjugated polymers is driven by
510 thermoelectric energy harvesting, as CVD polymers as thin as 2 nm have been incorporated into
511 nanostructured energy storage devices¹⁵⁵ to increase pseudocapacitive charge storage.
512 Selected examples of CVD polymer processing and applications are highlighted in **Fig. 6**.

513
514 Some, but not all, CVD polymerization methods use the same chemical reaction mechanisms
515 (step growth, chain growth, and condensation reactions) that underlie the synthesis of
516 polymers in solution (Table 4)¹³⁵. Low surface growth temperatures (typically in the range of -
517 10°C to 140°C) favor the adsorption of the CVD reactants, and traditional isotherms
518 quantitatively describe monomer uptake on the growth surface¹⁵⁶. Hence, knowledge of the
519 saturation pressure of a new vapour phase reactant at the growth temperature allows the
520 required CVD process conditions to be rapidly identified. This has been used for CVD growth of
521 hundreds of different homopolymers, copolymers, cross-linked organic networks, and
522 organic/inorganic films¹³⁶, with well-defined growth kinetics providing reproducible growth
523 even at sub-10 nm thickness¹⁴⁷. Alternatively, the CVD conditions can be adjusted for rapid
524 growth to produce films $> 10 \mu\text{m}$ thick¹⁵⁷.

525 Multiple strategies allow chemical covalent bonds to form between the substrate and the
526 growing CVD polymer layer¹³⁶. The resulting grafted interfaces greatly enhance durability.
527 Avoiding delamination [G] allows grafted CVD polymer films to be patterned and even to
528 survive sandblasting. Durability is also enhanced by using crosslinked monomers, as crosslinked
529 CVD organic networks display remarkable stability during multiple years of evaluation under
530 physiological conditions¹⁵⁸.

531 Fundamental understanding of CVD polymerization aids the scale-up to cost-effective
532 reactors >1 m in width and to economical roll-to-roll (R2R) processing¹³⁶, which is specifically
533 detailed below (Scaling up for factory-level applications). Properties can be tuned and optimized
534 through the selection of the volatile reactants and systematic variation of the CVD parameters
535 such as flow rates, pressure, and growth temperatures. Preserving the fidelity of the
536 monomeric structure in the polymer film is often key to optimizing properties. For example,
537 preserving the structure of the monomer 3,4-ethylene dioxythiophene (EDOT) by oCVD can
538 produce electrical conductivity >6000 S cm⁻¹¹⁵³. In contrast, plasma enhanced CVD does not
539 fully retain the chemical structure of EDOT and the resulting films typically have poor electrical
540 conductivity of <1 S cm⁻¹¹⁵².

541 [H2] Scaling up for factory-level applications

542 The rapid progress in CVD graphene synthesis technology means it is the first reported 2D
543 material to be scaled up at a factory level. While we have known for more than 50 years that
544 thin graphitic layers can be formed by CVD on nickel at high temperature using hydrocarbon
545 sources such as methane^{159,160}, these graphitic layers were not monolayers..owing to the high
546 carbon solubility of nickel during the CVD process. This problem was solved by thermally

547 depositing thin layers of nickel on SiO₂ substrates to limit the carbon concentration, leading to
548 the formation of centimeter-scale atomically thin layer of graphene^{39,65,161}. CVD graphene was
549 used to measure the **half integer quantum Hall effect [G]** originating from the ultra-high
550 mobility of charge carriers in graphene for the first time^{65,79}, implying that the electrical
551 performance of CVD graphene can be as good as mechanically exfoliated graphene. However,
552 the non-uniform segregation of carbon sources from nickel limits the crystallinity of CVD
553 graphene; this was overcome by using copper substrates that exhibit nearly zero carbon
554 solubility, where the graphene layer is formed by the Cu-mediated gradual surface diffusion
555 and crystallization of adsorbed carbon atoms^{38,160}. This self-limiting mechanism of graphene
556 growth immediately enabled the wafer-scale synthesis of monolayer graphene¹⁶², followed by
557 the meter-scale growth of monolayer graphene by employing continuous roll-to-roll (R2R)
558 methods¹⁶³. The large-area graphene synthesized by R2R technology has been utilized for
559 practical applications such as flexible touch screens for mobile phones, flexible OLEDs, flexible
560 transparent heaters, electromagnetic wave interference (EMI) shielding films, etc.^{36,164-166},
561 which are expected to be commercialized in the near future.

562 R2R synthesis and its continuous processes are essential for the industrial commercialization of
563 CVD graphene because it enables a >30-fold increase in productivity. These graphene synthesis
564 capabilities with respect to the advances in CVD technology are highlighted in **Fig. 7a**. While
565 plasma-assisted low-temperature growth is helpful to simplify the equipment setup and to save
566 electrical energy, it always results in poor graphene electrical conductivity because of high
567 defect density compared to graphene synthesized above 1,000 °C. In addition, putting multiple

568 copper sheets in a CVD chamber can increase synthesis capacity, but this type of batch
569 synthesis remains limited by long heating and cooling times. In the R2R system, time is not
570 wasted heating and cooling the CVD furnace; instead, the temperature in the furnace is kept
571 constant while the copper foils pass through the hot zone at a rate of $\sim 50\text{cm min}^{-1}$. R2R
572 synthesis was first proposed in 2010¹⁶³, while additional R2R systems employing slightly
573 different heater technologies were also developed^{23,35,167,168}. For example, a microwave plasma
574 technique was used to lower the synthesis temperature of the R2R process³⁵; 230 mm wide and
575 120 m long graphene films were synthesized by applying high current through copper foils
576 between the rolls¹⁶⁷; an open chamber system was used to enable the R2R synthesis of
577 graphene¹⁶⁹; a concentric CVD reactor was used for high-speed R2R manufacturing of graphene
578 films¹⁷⁰; and the 190 mm-wide vertical R2R system with rapid-thermal heaters enabled faster
579 and more homogeneous heating¹⁷¹. More recently, the development of 500 mm wide R2R
580 systems capable of synthesizing graphene on ~ 100 meters long Cu foils at the rate of ~ 500
581 $\text{mm} \cdot \text{min}^{-1}$ was reported¹⁷².

582 The R2R method allows for the application of vertical tension to single-crystallize the Cu foils
583 and achieve higher quality graphene films. It is also applicable to post-CVD processes including
584 etching and lamination (**Fig. 7b**), which are limited with batch-type CVD synthesis. R2R CVD
585 synthesis is therefore considered the best way to mass-produce the CVD graphene films for
586 commercial applications.

587 Although the scale-up for 2D materials synthesis is more complicated because it requires
588 multiple precursors in different phases, various CVD methods used for graphene synthesis have

589 been applied to the synthesis of other 2D materials. In general, powder sources are not
590 favorable for factory level synthesis of 2D materials because of the severe contamination of
591 reaction chambers by residual solids. Compared to conventional CVD methods using liquid or
592 solid precursors^{122,124}, MOCVD is anticipated to be the best route to synthesize high-
593 performance 2D materials larger than wafer scale¹⁷³. The R2R CVD method has demonstrated
594 the synthesis of MoS₂ films¹⁷⁴ as well as the synthesis of hBN film on metal foils¹⁷⁵. Atomic layer
595 deposition also appears as advantageous for the wafer-scale synthesis of high-mobility MoS₂ for
596 practical applications¹⁷⁶.

597 Since the CVD process is only one aspect of the full fabrication process to prepare graphene on
598 target substrates, the post-CVD processes including etching and transfer need to be equally
599 considered for factory level scale-up. For example, the continuous synthesis of graphene by R2R
600 methods must be followed by the R2R lamination of polymer supports¹⁶³, R2R removal of
601 copper foils by chemical etchant or electrochemical etching¹⁷⁵, and the patterning/transfer to
602 target substrates¹⁷⁷. The full R2R synthesis system is illustrated in **Fig. 8**.

603 [H1] Reproducibility and data deposition

604

605 The reproducibility and reliability of the performance of materials synthesized by CVD depends
606 on both the pre-treatment and post-CVD processes.

607 With respect to the pre-treatment of substrates, we shall take as an example copper foils
608 produced for general purposes. They are usually coated with an anti-oxidizing layer such as a
609 type of chrome oxide, which needs to be removed by acid or thermal treatment³⁶ before

610 graphene synthesis. In addition, these copper foils have usually been prepared by roll-pressing
611 and are polycrystalline; they must be recrystallized to obtain larger single-crystalline graphene
612 domains during deposition, as this is one of the crucial parameters minimizing defects and
613 maximizing electrical conductivity. One approach is to mechanically strain the Cu foil during
614 CVD to transform polycrystalline copper to copper with very large single crystal domains¹⁷⁸.
615 Since the graphene and Cu surfaces affect each other during growth, this causes the graphene-
616 covered region in Cu to undergo a drastic change in crystallinity¹⁷⁸. An alternative approach is to
617 prepare single-crystalline metal substrates by thermal annealing¹⁷⁹, an example of which is an
618 annealed monocrystalline Cu (110) substrate used to synthesize highly crystalline large-area *h*-
619 BN¹³⁰. Another example is molten gold, which at high temperature catalyzes the CVD growth of
620 single-crystalline *h*-BN, and where the small *h*-BN domains floating on the gold surface are
621 rotated by electrostatic interaction to commensurate each other to form a wafer-scale single
622 crystalline film¹⁸⁰.

623 The uniformity of 2D materials synthesized by CVD generally depend on the uniformity of
624 temperature and gas flow inside the reaction chamber³⁶. For example, in the case of graphene
625 synthesized by rapid thermal CVD, the temperature uniformity can be enhanced by using multi-
626 zone rapid thermal heaters, where more than 8 zones are separately controlled to balance the
627 temperature distribution (**Fig. 9a**). The use of graphite susceptors that convert optical radiation
628 to thermal energy is also useful to narrow down the temperature distribution. Most
629 importantly, automated control to exclude human error is the key to reproducibility (see the
630 less than 10% deviation of the graphene films sheet resistances from 10 different batches in
631 **Fig.9b** and their uniformity in **Fig 9c**, satisfying industrial requirements). The durability of the

632 electrical properties tested for industrial standard (85% humidity at 85 °C) was measured to be
633 suitable for practical applications (**Fig. 9d**).

634 As mentioned above, the CVD synthesis step is just one aspect of the full fabrication process,
635 so the post-CVD processes including etching and transfer are as important as the CVD process
636 to ensure reliability. In particular, the doping of graphene can increase the charge carrier
637 density and considerably lower sheet resistance, which is desirable for practical applications¹⁸¹.
638 In practice, the inhomogeneity and volatility of doping causes a reproducibility problem. The
639 elemental doping of graphene that replaces carbon atoms with boron or nitrogen atoms is very
640 stable and homogeneous, but it lowers charge carrier mobility due to electron scattering
641 around the heteroatoms¹⁸² and decreases electrical conductivity, which is undesirable. In
642 addition, while the non-destructive doping of graphene can be efficiently carried out by
643 molecular dopants and self-assembled monolayers¹⁸³⁻¹⁸⁵, it does not last long without proper
644 encapsulation¹⁸⁶⁻¹⁸⁸.

645 In summary, the reproducibility and reliability of the CVD-synthesized 2D materials largely
646 depends on the surface freshness and the crystallinity of the catalytic substrates as well as the
647 spatial uniformity of gas concentration and temperature, which need be considered in
648 designing CVD reactors.

649 [H1] Limitations and optimizations

650 The limitation of CVD technology often comes from the need for high temperature and high
651 vacuum, particularly for graphene and h-BN synthesis. The most common chamber materials
652 are quartz tubes that are thermally and mechanically strong enough to resist the reaction

653 conditions. As the quartz reactors are scalable only up to 12-inch (~30 cm) diameters, stainless-
654 steel chambers are alternatively used to design industrial scale CVD reactors, where advanced
655 chiller systems are essential to cool down the hot chamber and its housing. A quartz reactor is
656 advantageous because it is standardized and replaceable at relatively low cost whenever the
657 reactor is heavily contaminated. In contrast, a stainless steel reactor needs to be cleaned
658 periodically to keep the quality of synthesis. The growth of other 2D materials at mild
659 temperatures does not require quartz materials, but serious contamination of reaction
660 chambers is often caused by residual precursors. Thus, the use of replaceable quartz tubes and
661 gaseous precursors is recommended for 2D materials synthesis for industrial applications. In
662 addition, a plasma module can be combined to thermal CVD systems to lower the synthesis
663 temperature¹⁸⁹, but the high plasma energy often causes undesirable defects in the case of
664 graphene.

665 The weight of copper foils needs to be considered in the design of the R2R synthesis system.
666 The copper foil at ~1,000 °C becomes less stiff and more ductile, so the horizontal tension
667 across the 2~3 meters long rolls results in serious deformation. This can be minimized by
668 vertical loading parallel to the gravitational force and winding tension¹⁷⁸. In addition, the
669 vertical tension control is useful to promote the growth of single-crystalline Cu foils for high-
670 quality graphene synthesis¹⁷⁸.

671 To facilitate the optimization processes of CVD synthesis, high-throughput *in-situ* quality
672 assessment tools for graphene and 2D materials are of great importance. As CVD **often** involves
673 high temperatures and vacuum conditions, *in-situ* monitoring is possible only by an optical

674 method equipped with fiber and lens optics that can collect signals through the optical window
675 of CVD chambers. For this reason, Raman spectroscopy has been investigated as a
676 characterization tool to examine the number of layers, defect density, and coverage of
677 graphene and 2D materials¹⁰¹. However, its field of view and scanning speed are not large and
678 fast enough for factory-level real-time assessment, respectively. Wide-field Raman
679 spectroscopy that scans only D and G peak ranges is much faster, but it requires extremely
680 powerful laser sources incompatible with commercial instrumentation¹⁹⁰. Microwave
681 spectroscopy using eddy current¹⁹¹ and terahertz time-domain spectroscopy¹⁹² have enabled
682 the fast analysis of wafer scale graphene, but these methods are valid only for post-CVD
683 graphene transferred to insulating substrates. In terms of industrial quality control, the
684 evaluation of graphene as grown on copper foil is more important to optimize the growth
685 conditions. Confocal laser scanning microscopy (CLSM) is expected to satisfy the above-
686 mentioned demands for real-time assessment regardless of production scale¹⁹³. The CLSM
687 image contrast between graphene and copper substrate is found to be inversely proportional to
688 defect density, and therefore, the electrical conductivity can be briefly monitored by fast
689 scanning by CLSM (**Fig. 10**)¹⁷¹. It can be also applied to the quality assessment of other 2D
690 materials, although the laser wavelengths of CLSM need to be optimized on a case-by-case
691 basis.

692

693 [H1] Outlook

694 CVD reactors require relatively inexpensive components and are simple to set up, which has
695 led to their widespread use in the academic community for easily producing novel materials
696 such as graphene, 2D semiconductors and polymer thin films. However, CVD itself is a mature
697 commercial technology for applying thin films on variety of components and is particularly
698 useful in the electronics industry, where large area and continuous deposition of thin films can
699 be performed in specially designed reactors. Examples of these include vertical reactors for
700 floating catalytic synthesis of carbon nanotubes^{194,195} or R2R CVD systems for graphene
701 growth¹⁷⁸. The fundamental limitation of CVD is that it often requires high temperature
702 (typically >400 °C) to crack the precursors into reactive products that can readily form thin films
703 (especially for graphene and *h*BN). Lower deposition temperatures can be achieved by utilising
704 plasma to produce excited state or ionised precursors that can react at low temperatures. The
705 ability to deposit high quality films at low temperatures (typically <400 °C) is highly desirable in
706 back-end-of-the-line processes for electronics, thermosensitive substrates, and soft metals. The
707 critical challenges that remain in low temperature CVD for growing inorganic materials are lack
708 of crystallinity, trapped precursors, and maintenance of the desired stoichiometry.

709 CVD is the most widely used method for large area synthesis of advanced low-dimensional
710 materials such as nanowires, nanotubes, and more recently two-dimensional materials, and is
711 exclusively used for large area synthesis of graphene. While very high-quality graphene films
712 can now be achieved over meter scales using CVD, a remaining challenge is that the growth is
713 limited to copper (or its alloy). This is a challenge because in order to use graphene for

714 electronics, optics and other applications, it must be transferred onto a desired substrate. A
715 substantial amount of research has been devoted to clean transfer of graphene from copper
716 onto arbitrary substrates. This research has led to substantial progress and demonstrations that
717 high quality graphene can be transferred onto virtually any substrate. However, the risk of tears
718 and wrinkles along with incorporation of copper or transfer solvent impurities remain. Thus,
719 research in contamination and damage free transfer must continue. The ultimate achievement
720 for CVD of graphene would be the development of a process that allows direct growth of
721 graphene on any substrate. In particular, the direct, large area and local growth of graphene on
722 insulating wafers used in electronics would be a major breakthrough.

723 The research in 2D semiconductors – in particular TMDs – has clearly shown that they hold
724 tremendous promise for electronics and other applications. A major bottleneck for their
725 implementation is that the absence of a CVD process that allows the realisation of high-quality
726 large area (for example, wafer scale) thin films. The advantage of TMD films – in contrast to
727 graphene growth – is that they can be directly grown on insulating substrates but centimetre-
728 scale single crystal (or even large grained) thin films are still challenging. MOCVD has shown
729 promise in achieving uniform wafer-scale atomically thin films of semiconducting 2D materials
730 such as MoS₂ and WS₂ with nanoscale domain sizes, but additional work is needed to increase
731 the size of the crystals in the atomically thin films and minimise the concentration of grain
732 boundaries. Uniform growth of single crystal 2D thin films therefore requires knowledge of the
733 nucleation and growth mechanisms that must be established through detailed analyses of the
734 reactive gas phase, surface phenomena, and measurements during MOCVD growth. In addition

735 to semiconducting 2D materials, metallic compounds (such as NbS₂ and VS₂) are interesting
736 from both fundamental and technological viewpoints, because high quality metallic 2D
737 compounds synthesized via MOCVD could hold promise for high-performance contacts and
738 interconnects. Another interesting direction of research in 2D semiconductors is the integration
739 of different materials by stacking. To exploit the optoelectronic properties of vertically stacked
740 heterostructures, different TMD layers must be grown on each other. Some preliminary results
741 suggest that this is possible but more work is needed to realise wafer scale stacked 2D layers.

742 A fundamental problem that is rarely discussed in CVD of 2D semiconductors – in particular
743 TMDs – is that high-temperature deposition and subsequent cooling leads to by-products of
744 chalcogen (S, Se, Te) species (for example, sub-stoichiometric compounds). Decreasing the
745 temperature compromises the crystalline quality of the TMD films. Thus, development of
746 deposition and cooling processes are required to ensure that the deposited atomically thin
747 films are indeed stoichiometric. Finally, the dearth of MOCVD precursors means that only a
748 handful of 2D semiconductor compounds can be grown. This means that many interesting TMD
749 compounds – in particular metallic ones – cannot currently be deposited by MOCVD. Efforts to
750 expand the number and type of precursors will benefit the growth community in realising new
751 compounds as well as perfecting the growth of existing capabilities. A challenge with MOCVD is
752 that the precursors are toxic and thus specialized spaces with appropriate safety precautions
753 are needed to carry out the experiments. Development of benign precursors could also lead to
754 more widespread adoption of MOCVD and accelerate the development of 2D thin films.

755 To summarize, the key challenges to be addressed in CVD of 2D materials are: lowering the
756 deposition temperature; uniform and large area growth on a variety of substrates; and
757 developing benign precursors for MOCVD growth of a wide range of TMD materials.

758 In this Primer, we have presented a comprehensive overview of CVD methods. We have
759 included the instrument construction and the process of material preparation and
760 characterization, concentrating on the growth of graphene and other 2D materials such as
761 TMDs and polymeric thin films. The recent advances and challenges of this technique in terms
762 of mass-production, controllability, reproducibility, cost and online-monitoring have also been
763 highlighted, in the hope of underscoring the importance and benefit CVD can bring to modern
764 industry.

765

766

767
768
769
770
771
772
773
774
775
776
777
778
779
780
781
782
783
784
785
786
787
788
789
790
791
792
793
794
795
796
797
798
799
800
801
802
803
804
805
806
807
808
809
810
811
812
813
814
815
816
817
818
819
820

References:

1. Teal, G. K., Fisher, J. R. & Treptow, A. W. A New Bridge Photo - Cell Employing a Photo - Conductive Effect in Silicon. Some Properties of High Purity Silicon. *Journal of Applied Physics* **17**, 879-886 (1946).
2. Carlson, D. E. & Wronski, C. R. Amorphous silicon solar cell. *Appl Phys Lett* **28**, 671-673 (1976).
3. Knights, J. C. Substitutional doping in amorphous silicon. *American Institute of Physics Conference Series* **31**, 296-300 (1976).
4. Manasevit, H. M. Recollections and reflections of MO-CVD. *Journal of Crystal Growth* **55**, 1-9 (1981).
5. Tsang, W. T. Chemical beam epitaxy of InP and GaAs. *Appl Phys Lett* **45**, 1234-1236 (1984).
6. Xia, Y. *et al.* One-Dimensional Nanostructures: Synthesis, Characterization, and Applications. *Advanced Materials* **15**, 353-389 (2003).
7. Novoselov, K. S. *et al.* Electric field effect in atomically thin carbon films. *Science* **306**, 666-669 (2004).
8. Novoselov, K. S. *et al.* A roadmap for graphene. *Nature* **490**, 192-200 (2012).
9. Lin, L., Deng, B., Sun, J., Peng, H. & Liu, Z. Bridging the Gap between Reality and Ideal in Chemical Vapor Deposition Growth of Graphene. *Chem Rev* **118**, 9281-9343 (2018).
- This review provides a systematic introduction to the CVD growth of graphene.**
10. Choy, K. L. Chemical vapour deposition of coatings. *Progress in Materials Science* **48**, 57-170 (2003).
11. Yan, K., Fu, L., Peng, H. L. & Liu, Z. F. Designed CVD Growth of Graphene via Process Engineering. *Accounts Chem Res* **46**, 2263-2274 (2013).
12. Wang, H. *et al.* Primary Nucleation-Dominated Chemical Vapor Deposition Growth for Uniform Graphene Monolayers on Dielectric Substrate. *J Am Chem Soc* **141**, 11004-11008 (2019).
13. Xie, H. *et al.* H₂O-Etchant-Promoted Synthesis of High-Quality Graphene on Glass and Its Application in See-Through Thermochromic Displays. *Small* **16**, e1905485 (2020).
14. Park, J. H. *et al.* Large-Area Monolayer Hexagonal Boron Nitride on Pt Foil. *ACS Nano* **8**, 8520-8528 (2014).
15. Zhang, Z. W. *et al.* Robust epitaxial growth of two-dimensional heterostructures, multiheterostructures, and superlattices. *Science* **357**, 788+ (2017).
16. Sahoo, P. K., Memaran, S., Xin, Y., Balicas, L. & Gutierrez, H. R. One-pot growth of two-dimensional lateral heterostructures via sequential edge-epitaxy. *Nature* **553**, 63-67 (2018).
17. Ji, Q. *et al.* Epitaxial monolayer MoS₂ on mica with novel photoluminescence. *Nano Lett* **13**, 3870-3877 (2013).
18. Zhang, Y. *et al.* Controlled Growth of High-Quality Monolayer WS₂ Layers on Sapphire and Imaging Its Grain Boundary. *ACS Nano* **7**, 8963-8971 (2013).
19. Wu, J. *et al.* Controlled Synthesis of High-Mobility Atomically Thin Bismuth Oxyselenide Crystals. *Nano Lett* **17**, 3021-3026 (2017).
20. Jia, K. C. *et al.* Copper-Containing Carbon Feedstock for Growing Superclean Graphene. *J. Am. Chem. Soc.* **141**, 7670-7674 (2019).
21. Wang, H. *et al.* Synthesis of boron-doped graphene monolayers using the sole solid feedstock by chemical vapor deposition. *Small* **9**, 1316-1320 (2013).
22. Jiang, B. *et al.* Batch synthesis of transfer-free graphene with wafer-scale uniformity. *Nano Research* (2020).
23. Deng, B. *et al.* Roll-to-Roll Encapsulation of Metal Nanowires between Graphene and Plastic Substrate for High-Performance Flexible Transparent Electrodes. *Nano Lett* **15**, 4206-4213 (2015).
25. Deng, B. *et al.* Scalable and ultrafast epitaxial growth of single-crystal graphene wafers for electrically tunable liquid-crystal microlens arrays. *Science Bulletin* **64**, 659-668 (2019).
26. Tang, L. *et al.* Vertical Chemical Vapor Deposition Growth of Highly Uniform 2D Transition Metal Dichalcogenides. *ACS Nano* (2020).
27. Xu, J. *et al.* Fast Batch Production of High-Quality Graphene Films in a Sealed Thermal Molecular Movement System. *Small* **13**, 1700651 (2017).
28. Li, Y. *et al.* Large Single-Crystal Cu Foils with High-Index Facets by Strain-Engineered Anomalous Grain Growth. *Adv Mater*, e2002034 (2020).
29. Deng, B., Liu, Z. & Peng, H. Toward Mass Production of CVD Graphene Films. *Adv Mater*, e1800996 (2018).
30. Chen, X. D. *et al.* Fast Growth and Broad Applications of 25-Inch Uniform Graphene Glass. *Adv Mater* **29** (2017).

- 821 31. Sun, Z. Z. *et al.* Large-Area Bernal-Stacked Bi-, Tr-, and Tetralayer Graphene. *ACS Nano* **6**, 9790-9796
822 (2012).
- 823 32. Xu, Y. & Yan, X.-T. *Chemical Vapour Deposition An Integrated Engineering Design for Advanced*
824 *Materials*. (Springer, 2010).
- 825 33. Bointon, T. H., Barnes, M. D., Russo, S. & Craciun, M. F. High Quality Monolayer Graphene Synthesized
826 by Resistive Heating Cold Wall Chemical Vapor Deposition. *Advanced Materials* **27**, 4200-4206 (2015).
- 827 34. Qi, Y. *et al.* Switching Vertical to Horizontal Graphene Growth Using Faraday Cage-Assisted PECVD
828 Approach for High-Performance Transparent Heating Device. *Adv Mater* **30** (2018).
- 829 35. Yamada, T., Ishihara, M., Kim, J., Hasegawa, M. & Iijima, S. A roll-to-roll microwave plasma chemical
830 vapor deposition process for the production of 294mm width graphene films at low temperature. *Carbon* **50**,
831 2615-2619 (2012).
- 832 36. Ryu, J. *et al.* Fast Synthesis of High-Performance Graphene Films by Hydrogen-Free Rapid Thermal
833 Chemical Vapor Deposition. *ACS Nano* **8**, 950-956 (2014).
- 834 37. Piner, R. *et al.* Graphene Synthesis via Magnetic Inductive Heating of Copper Substrates. *ACS Nano* **7**,
835 7495-7499 (2013).
- 836 38. Li, X. *et al.* Large-Area Synthesis of High-Quality and Uniform Graphene Films on Copper Foils. *Science*
837 **324**, 1312 (2009).
- 838 **This is the first report of large-area monolayer graphene films via CVD.**
- 839 39. Reina, A. *et al.* Large Area, Few-Layer Graphene Films on Arbitrary Substrates by Chemical Vapor
840 Deposition. *Nano Lett* **9**, 30-35 (2009).
- 841 40. Chen, J. *et al.* Oxygen-aided synthesis of polycrystalline graphene on silicon dioxide substrates. *J Am*
842 *Chem Soc* **133**, 17548-17551 (2011).
- 843 41. Chen, Z. *et al.* High-Brightness Blue Light-Emitting Diodes Enabled by a Directly Grown Graphene Buffer
844 Layer. *Adv Mater* **30**, e1801608 (2018).
- 845 42. Chen, Z., Qi, Y., Chen, X., Zhang, Y. & Liu, Z. Direct CVD Growth of Graphene on Traditional Glass:
846 Methods and Mechanisms. *Adv Mater* **31**, e1803639 (2019).
- 847 43. Hao, Y. F. *et al.* The Role of Surface Oxygen in the Growth of Large Single-Crystal Graphene on Copper.
848 *Science* **342**, 720-723 (2013).
- 849 44. Sun, L. *et al.* Visualizing fast growth of large single-crystalline graphene by tunable isotopic carbon source.
850 *Nano Res.* **10**, 355-363 (2016).
- 851 45. Xu, X. *et al.* Ultrafast epitaxial growth of metre-sized single-crystal graphene on industrial Cu foil. *Science*
852 *Bulletin* **62**, 1074-1080 (2017).
- 853 **This report highlights the transformation of polycrystalline metal foil to a single-crystal one for high-**
854 **quality graphene growth.**
- 855 46. Wu, M. *et al.* Seeded growth of large single-crystal copper foils with high-index facets. *Nature* **581**, 406-
856 410 (2020).
- 857 47. Li, Y., Sun, L., Liu, H., Wang, Y. & Liu, Z. Preparation of single-crystal metal substrates for growth of
858 high-quality two-dimensional materials. *Inorg. Chem. Front.*, 10.1039/D1030QI00923G (2020).
- 859 48. German, E. D. & Sheintuch, M. Predicting CH₄ Dissociation Kinetics on Metals: Trends, Sticking
860 Coefficients, H Tunneling, and Kinetic Isotope Effect. *J Phys Chem C* **117**, 22811-22826 (2013).
- 861 49. Li, X. S. *et al.* Graphene Films with Large Domain Size by a Two-Step Chemical Vapor Deposition
862 Process. *Nano Lett.* **10**, 4328-4334 (2010).
- 863 50. Bhaviripudi, S., Jia, X., Dresselhaus, M. S. & Kong, J. Role of kinetic factors in chemical vapor deposition
864 synthesis of uniform large area graphene using copper catalyst. *Nano Lett* **10**, 4128-4133 (2010).
- 865 51. Lin, L. *et al.* Towards super-clean graphene. *Nat Commun* **10**, 1912 (2019).
- 866 52. Sun, J. *et al.* Direct Chemical Vapor Deposition-Derived Graphene Glasses Targeting Wide Ranged
867 Applications. *Nano Lett* **15**, 5846-5854 (2015).
- 868 53. Li, X. S., Cai, W. W., Colombo, L. & Ruoff, R. S. Evolution of Graphene Growth on Ni and Cu by Carbon
869 Isotope Labeling. *Nano Lett.* **9**, 4268-4272 (2009).
- 870 54. Dai, B. *et al.* Rational design of a binary metal alloy for chemical vapour deposition growth of uniform
871 single-layer graphene. *Nat Commun* **2**, 522 (2011).
- 872 55. Liu, X. *et al.* Segregation Growth of Graphene on Cu-Ni Alloy for Precise Layer Control. *The Journal of*
873 *Physical Chemistry C* **115**, 11976-11982 (2011).
- 874 56. Liu, N. *et al.* The origin of wrinkles on transferred graphene. *Nano Research* **4**, 996-1004 (2011).

- 875 57. Deng, B. *et al.* Wrinkle-Free Single-Crystal Graphene Wafer Grown on Strain-Engineered Substrates. *ACS*
876 *Nano* **11**, 12337-12345 (2017).
- 877 58. Zhang, C., Fu, L., Zhang, Y. & Liu, Z. Segregation Phenomenon and Its Control in the Catalytic Growth of
878 Graphene. *Acta Chimica Sinica* **71**, 308-308 (2013).
- 879 59. Deng, B. *et al.* Anisotropic Strain Relaxation of Graphene by Corrugation on Copper Crystal Surfaces.
880 *Small* **14**, e1800725 (2018).
- 881 60. Massalski, T. B., Murray, J. L., Bennet, L. H. & Baker, H. *Binary alloy phase diagrams*. (ASM
882 International, 1986).
- 883 61. Dwight E. Gray, A. I. o. P. *American Institute of Physics Handbook*. Third edit edn, (Mcgraw-Hill Book
884 Company, 1972).
- 885 62. Reina, A. *et al.* Growth of Large-Area Single- and Bi-Layer Graphene by Controlled Carbon Precipitation
886 on Polycrystalline Ni Surfaces. *Nano Res.* **2**, 509-516 (2009).
- 887 63. Yan, K. *et al.* Modulation-doped growth of mosaic graphene with single-crystalline p-n junctions for
888 efficient photocurrent generation. *Nat Commun* **3**, 1280 (2012).
- 889 64. Blake, P. *et al.* Making graphene visible. *Appl Phys Lett* **91**, 063124 (2007).
- 890 65. Kim, K. S. *et al.* Large-scale pattern growth of graphene films for stretchable transparent electrodes. *Nature*
891 **457**, 706-710 (2009).
- 892 66. Huang, M. *et al.* Large-area single-crystal AB-bilayer and ABA-trilayer graphene grown on a Cu/Ni(111)
893 foil. *Nat Nanotechnol* **15**, 289-295 (2020).
- 894 67. Gao, L. B. *et al.* Repeated growth and bubbling transfer of graphene with millimetre-size single-crystal
895 grains using platinum. *Nat Commun* **3**, 699 (2012).
- 896 69. Duong, D. L. *et al.* Probing graphene grain boundaries with optical microscopy. *Nature* **490**, 235-239
897 (2012).
- 898 70. Gan, L. & Luo, Z. T. Turning off Hydrogen To Realize Seeded Growth of Subcentimeter Single-Crystal
899 Graphene Grains on Copper. *ACS Nano* **7**, 9480-9488 (2013).
- 900 71. Ly, T. H. *et al.* Nondestructive Characterization of Graphene Defects. *Adv Funct Mater* **23**, 5183-5189
901 (2013).
- 902 72. Kong, X. H. *et al.* Non-destructive and rapid evaluation of chemical vapor deposition graphene by dark
903 field optical microscopy. *Appl Phys Lett* **103**, 043119 (2013).
- 904 73. Huang, L. *et al.* Twinkling graphene on polycrystalline Cu substrate: A scanning electron microscopy study.
905 *Journal of Applied Physics* **125** (2019).
- 906 74. Huang, L. *et al.* High-Contrast SEM Imaging of Supported Few-Layer Graphene for Differentiating
907 Distinct Layers and Resolving Fine Features: There is Plenty of Room at the Bottom. *Small* **14**, e1704190
908 (2018).
- 909 75. Wang, Z. J. *et al.* Direct Observation of Graphene Growth and Associated Copper Substrate Dynamics by
910 in Situ Scanning Electron Microscopy. *ACS Nano* **9**, 1506-1519 (2015).
- 911 76. Lee, C., Wei, X. D., Kysar, J. W. & Hone, J. Measurement of the elastic properties and intrinsic strength of
912 monolayer graphene. *Science* **321**, 385-388 (2008).
- 913 77. Sun, L. *et al.* A Force-Engineered Lint Roller for Superclean Graphene. *Adv Mater* **31**, 1902978 (2019).
- 914 78. Kang, J. H. *et al.* Strain Relaxation of Graphene Layers by Cu Surface Roughening. *Nano Lett* **16**, 5993-
915 5998 (2016).
- 916 79. Bae, S. *et al.* Roll-to-roll production of 30-inch graphene films for transparent electrodes. *Nat Nanotechnol*
917 **5**, 574-578 (2010).
- 918 **This report highlights the large-scale growth and transfer of graphene films.**
- 919 80. Yu, Q. K. *et al.* Control and characterization of individual grains and grain boundaries in graphene grown
920 by chemical vapour deposition. *Nat Mater* **10**, 443-449 (2011).
- 921 81. Levy, N. *et al.* Strain-Induced Pseudo-Magnetic Fields Greater Than 300 Tesla in Graphene Nanobubbles.
922 *Science* **329**, 544-547 (2010).
- 923 82. Lahiri, J., Lin, Y., Bozkurt, P., Oleynik, I. I. & Batzill, M. An extended defect in graphene as a metallic
924 wire. *Nat Nanotechnol* **5**, 326-329 (2010).
- 925 83. Artyukhov, V. I., Liu, Y. Y. & Yakobson, B. I. Equilibrium at the edge and atomistic mechanisms of
926 graphene growth. *P Natl Acad Sci USA* **109**, 15136-15140 (2012).
- 927 84. Shu, H. B., Chen, X. S., Tao, X. M. & Ding, F. Edge Structural Stability and Kinetics of Graphene
928 Chemical Vapor Deposition Growth. *ACS Nano* **6**, 3243-3250 (2012).

- 929 85. Yuan, Q. H. *et al.* Magic Carbon Clusters in the Chemical Vapor Deposition Growth of Graphene. *J. Am.*
930 *Chem. Soc.* **134**, 2970-2975 (2012).
- 931 86. Rasool, H. I. *et al.* Continuity of Graphene on Polycrystalline Copper. *Nano Lett* **11**, 251-256 (2011).
- 932 87. Rasool, H. I. *et al.* Atomic-Scale Characterization of Graphene Grown on Copper (100) Single Crystals. *J*
933 *Am Chem Soc* **133**, 12536-12543 (2011).
- 934 88. Yang, W. *et al.* Epitaxial growth of single-domain graphene on hexagonal boron nitride. *Nat Mater* **12**,
935 792-797 (2013).
- 936 89. Liu, L. *et al.* Heteroepitaxial Growth of Two-Dimensional Hexagonal Boron Nitride Templated by
937 Graphene Edges. *Science* **343**, 163-167 (2014).
- 938 90. Yuan, G. W. *et al.* Proton-assisted growth of ultra-flat graphene films. *Nature* **577**, 204-208 (2020).
- 939 91. Sutter, E., Acharya, D. P., Sadowski, J. T. & Sutter, P. Scanning tunneling microscopy on epitaxial bilayer
940 graphene on ruthenium (0001). *Appl Phys Lett* **94**, 133101 (2009).
- 941 92. Gao, L., Guest, J. R. & Guisinger, N. P. Epitaxial Graphene on Cu(111). *Nano Lett* **10**, 3512-3516 (2010).
- 942 93. Hashimoto, A., Suenaga, K., Gloter, A., Urita, K. & Iijima, S. Direct evidence for atomic defects in
943 graphene layers. *Nature* **430**, 870-873 (2004).
- 944 94. Huang, P. Y. *et al.* Grains and grain boundaries in single-layer graphene atomic patchwork quilts. *Nature*
945 **469**, 389-392 (2011).
- 946 95. Kim, K. *et al.* Grain Boundary Mapping in Polycrystalline Graphene. *ACS Nano* **5**, 2142-2146 (2011).
- 947 96. Lee, J. H. *et al.* Wafer-Scale Growth of Single-Crystal Monolayer Graphene on Reusable Hydrogen-
948 Terminated Germanium. *Science* **344**, 286-289 (2014).
- 949 97. Jiang, Y. *et al.* Electron ptychography of 2D materials to deep sub-angstrom resolution. *Nature* **559**, 343-
950 349 (2018).
- 951 98. Chen, T. A. *et al.* Wafer-scale single-crystal hexagonal boron nitride monolayers on Cu (111). *Nature* **579**,
952 219-223 (2020).
- 953 100. Xu, X. Z. *et al.* Ultrafast growth of single-crystal graphene assisted by a continuous oxygen supply. *Nat*
954 *Nanotechnol* **11**, 930-935 (2016).
- 955 101. Ferrari, A. C. & Basko, D. M. Raman spectroscopy as a versatile tool for studying the properties of
956 graphene. *Nat Nanotechnol* **8**, 235-246 (2013).
- 957 **This paper highlights the utility of Raman spectroscopy for characterizing the properties of graphene.8**
- 958 102. Ferrari, A. C. *et al.* Raman spectrum of graphene and graphene layers. *Phys Rev Lett* **97**, 187401 (2006).
- 959 103. Das, A. *et al.* Monitoring dopants by Raman scattering in an electrochemically top-gated graphene
960 transistor. *Nat Nanotechnol* **3**, 210-215 (2008).
- 961 104. Lee, J. E., Ahn, G., Shim, J., Lee, Y. S. & Ryu, S. Optical separation of mechanical strain from charge
962 doping in graphene. *Nat Commun* **3**, 1024 (2012).
- 963 105. Bronsgeest, M. S. *et al.* Strain Relaxation in CVD Graphene: Wrinkling with Shear Lag. *Nano Lett* **15**,
964 5098-5104 (2015).
- 965 106. Zhao, T. *et al.* Ultrafast growth of nanocrystalline graphene films by quenching and grain-size-dependent
966 strength and bandgap opening. *Nat Commun* **10**, 4854 (2019).
- 967 107. Varykhalov, A. *et al.* Electronic and Magnetic Properties of Quasifreestanding Graphene on Ni. *Phys Rev*
968 *Lett* **101**, 157601 (2008).
- 969 108. Avila, J. *et al.* Exploring electronic structure of one-atom thick polycrystalline graphene films: A nano
970 angle resolved photoemission study. *Sci Rep-Uk* **3**, 2439 (2013).
- 971 109. Varykhalov, A., Scholz, M. R., Kim, T. K. & Rader, O. Effect of noble-metal contacts on doping and band
972 gap of graphene. *Phys Rev B* **82**, 121101 (2010).
- 973 110. Gottardi, S. *et al.* Comparing Graphene Growth on Cu(111) versus Oxidized Cu(111). *Nano Lett* **15**, 917-
974 922 (2015).
- 975 111. Bakharev, P. V. *et al.* Chemically induced transformation of chemical vapour deposition grown bilayer
976 graphene into fluorinated single-layer diamond. *Nat Nanotechnol* **15**, 59-66 (2020).
- 977 112. Zhan, Y., Liu, Z., Najmaei, S., Ajayan, P. M. & Lou, J. Large-Area Vapor-Phase Growth and
978 Characterization of MoS₂ Atomic Layers on a SiO₂ Substrate. *Small* **8**, 966-971 (2012).
- 979 113. Chhowalla, M., Liu, Z. & Zhang, H. Two-dimensional transition metal dichalcogenide (TMD) nanosheets.
980 *Chemical Society Reviews* **44**, 2584-2586 (2015).
- 981 **This review article introduces two-dimensional transition metal dichalcogenides.**
- 982 114. Lv, R. *et al.* Transition Metal Dichalcogenides and Beyond: Synthesis, Properties, and Applications of
983 Single- and Few-Layer Nanosheets. *Accounts of Chemical Research* **48**, 56-64 (2015).

- 984 115. Liu, K.-K. *et al.* Growth of Large-Area and Highly Crystalline MoS₂ Thin Layers on Insulating Substrates. *Nano Lett* **12**, 1538-1544 (2012).
- 985
- 986 116. Wang, X. *et al.* Chemical Vapor Deposition Growth of Crystalline Monolayer MoSe₂. *ACS Nano* **8**, 5125-5131 (2014).
- 987
- 988 117. Huang, C. *et al.* Lateral heterojunctions within monolayer MoSe₂-WSe₂ semiconductors. *Nat Mater* **13**, 1096-1101 (2014).
- 989
- 990 118. Liu, B. *et al.* Chemical Vapor Deposition Growth of Monolayer WSe₂ with Tunable Device Characteristics and Growth Mechanism Study. *ACS Nano* **9**, 6119-6127 (2015).
- 991
- 992 119. Li, S. *et al.* Halide-assisted atmospheric pressure growth of large WSe₂ and WS₂ monolayer crystals. *Applied Materials Today* **1**, 60-66 (2015).
- 993
- 994 120. Li, G. *et al.* Direct Growth of Continuous and Uniform MoS₂ Film on SiO₂/Si Substrate Catalyzed by Sodium Sulfate. *The Journal of Physical Chemistry Letters* **11**, 1570-1577 (2020).
- 995
- 996 121. Yang, P. *et al.* Batch production of 6-inch uniform monolayer molybdenum disulfide catalyzed by sodium in glass. *Nat Commun* **9**, 979 (2018).
- 997
- 998 122. Lee, Y.-H. *et al.* Synthesis of Large-Area MoS₂ Atomic Layers with Chemical Vapor Deposition. *Advanced Materials* **24**, 2320-2325 (2012).
- 999
- 1000 123. Dumcenco, D. *et al.* Large-Area Epitaxial Monolayer MoS₂. *ACS Nano* **9**, 4611-4620 (2015).
- 1001 124. Kang, K. *et al.* High-mobility three-atom-thick semiconducting films with wafer-scale homogeneity. *Nature* **520**, 656-660 (2015).
- 1002
- 1003 125. Kim, H., Ovchinnikov, D., Deiana, D., Unuchek, D. & Kis, A. Suppressing Nucleation in Metal-Organic Chemical Vapor Deposition of MoS₂ Monolayers by Alkali Metal Halides. *Nano Lett* **17**, 5056-5063 (2017).
- 1004
- 1005
- 1006 126. Wang, Y. *et al.* Van der Waals contacts between three-dimensional metals and two-dimensional semiconductors. *Nature* **568**, 70-74 (2019).
- 1007
- 1008 127. Zhou, J. *et al.* A library of atomically thin metal chalcogenides. *Nature* **556**, 355-359 (2018).
- 1009 128. Yang, J. *et al.* Ultrahigh-current-density niobium disulfide catalysts for hydrogen evolution. *Nat Mater* **18**, 1309-1314 (2019).
- 1010
- 1011 129. Behura, S., Nguyen, P., Che, S., Debbarma, R. & Berry, V. Large-Area, Transfer-Free, Oxide-Assisted Synthesis of Hexagonal Boron Nitride Films and Their Heterostructures with MoS₂ and WS₂. *J Am Chem Soc* **137**, 13060-13065 (2015).
- 1012
- 1013
- 1014 130. Wang, L. *et al.* Epitaxial growth of a 100-square-centimetre single-crystal hexagonal boron nitride monolayer on copper. *Nature* **570**, 91-95 (2019).
- 1015
- 1016 131. Xu, C. *et al.* Large-area high-quality 2D ultrathin Mo₂C superconducting crystals. *Nat Mater* **14**, 1135-1141 (2015).
- 1017
- 1018 132. Wang, Z. *et al.* Metal Immiscibility Route to Synthesis of Ultrathin Carbides, Borides, and Nitrides. *Adv Mater* **29** (2017).
- 1019
- 1020 133. Wu, J. *et al.* High electron mobility and quantum oscillations in non-encapsulated ultrathin semiconducting Bi₂O₂Se. *Nat Nanotechnol* (2017).
- 1021
- 1022 134. Tan, C. *et al.* Wafer-Scale Growth of Single-Crystal 2D Semiconductor on Perovskite Oxides for High-Performance Transistors. *Nano Lett* **19**, 2148-2153 (2019).
- 1023
- 1024 135. Gleason, K. K. *CVD Polymers: Fabrication of Organic Surfaces and Devices*. 1-461 (John Wiley & Sons, 2015).
- 1025
- 1026 136. Gleason, K. K. Nanoscale control by chemically vapour-deposited polymers. *Nat. Rev. Phys.* **2**, 347-364 (2020).
- 1027
- 1028 **This review introduces the controllable growth of polymers via CVD.**
- 1029 137. De Luna, M. M., Karandikar, P. & Gupta, M. Interactions between polymers and liquids during initiated chemical vapor deposition onto liquid substrates. *Mol. Syst. Des. Eng.* **5**, 15-21 (2020).
- 1030
- 1031 138. Donadt, T. B. & Yang, R. Vapor-Deposited Biointerfaces and Bacteria: An Evolving Conversation. *ACS Biomaterials Science & Engineering* **6**, 182-197 (2020).
- 1032
- 1033 139. Moni, P., Al-Obeidi, A. & Gleason, K. K. Vapor deposition routes to conformal polymer thin films. *Beilstein Journal of Nanotechnology* **8**, 723-735 (2017).
- 1034
- 1035 140. Coclite, A. M. Smart surfaces by initiated chemical vapor deposition. *Surface innovations* **1**, 6-14 (2013).
- 1036 141. Gleason, K. K. Chemically vapor deposited polymer nanolayers for rapid and controlled permeation of molecules and ions. *Journal of Vacuum Science & Technology A: Vacuum, Surfaces, and Films* **38**, 020801 (2020).
- 1037
- 1038

- 1039 142. Perrotta, A., Werzer, O. & Coclite, A. M. Strategies for Drug Encapsulation and Controlled Delivery Based
1040 on Vapor - Phase Deposited Thin Films. *Advanced Engineering Materials* **20**, 1700639 (2018).
- 1041 143. Sayin, S., Ozdemir, E., Acar, E. & Ince, G. O. Multifunctional one-dimensional polymeric nanostructures
1042 for drug delivery and biosensor applications. *Nanotechnology* **30**, 412001 (2019).
- 1043 144. Zhao, J. & Gleason, K. K. Solvent-less vapor-phase fabrication of membranes for sustainable separation
1044 processes. *Engineering* (2020).
- 1045 145. Lewis, H. G. P., Bansal, N. P., White, A. J. & Handy, E. S. HWCVD of polymers: Commercialization and
1046 scale-up. *Thin Solid Films* **517**, 3551-3554 (2009).
- 1047 146. Kim, S. *et al.* Ultrathin high-resolution flexographic printing using nanoporous stamps. *Science Advances* **2**,
1048 e1601660 (2016).
- 1049 147. Suh, H. S. *et al.* Sub-10-nm patterning via directed self-assembly of block copolymer films with a vapour-
1050 phase deposited topcoat. *Nat Nanotechnol* **12**, 575 (2017).
- 1051 148. Moni, P. *et al.* Ultrathin and Conformal Initiated Chemical-Vapor-Deposited Layers of Systematically
1052 Varied Surface Energy for Controlling the Directed Self-Assembly of Block CoPolymers. *Langmuir* **34**,
1053 4494-4502 (2018).
- 1054 149. Yang, G. G. *et al.* Conformal 3D Nanopatterning by Block Copolymer Lithography with Vapor-Phase
1055 Deposited Neutral Adlayer. *ACS Nano* **13**, 13092-13099 (2019).
- 1056 150. Yu, S. J. *et al.* Initiated chemical vapor deposition: A versatile tool for various device applications.
1057 *Advanced Engineering Materials* **20**, 1700622 (2018).
- 1058 **This review article highlights the synthesis of polymers via an advanced CVD method.**
- 1059 151. Kim, J. H. *et al.* in *2018 IEEE International Electron Devices Meeting (IEDM)*. 11.11. 11-11.11. 14
1060 (IEEE).
- 1061 152. Gharahcheshmeh, M. H. & Gleason, K. K. Device fabrication based on oxidative chemical vapor
1062 deposition (oCVD) synthesis of conducting polymers and related conjugated organic materials. *Advanced*
1063 *Materials Interfaces* **6**, 1801564 (2019).
- 1064 153. Wang, X. *et al.* High electrical conductivity and carrier mobility in oCVD PEDOT thin films by engineered
1065 crystallization and acid treatment. *Science advances* **4**, eaat5780 (2018).
- 1066 **The electrical conductivity and carrier mobility of a mechanically flexible CVD organic polymer thin**
1067 **film reaches the levels found in mechanical brittle indium tin oxide.**
- 1068 154. Gueye, M. N., Carella, A., Faure-Vincent, J., Demadrille, R. & Simonato, J.-P. Progress in understanding
1069 structure and transport properties of PEDOT-based materials: A critical review. *Progress in Materials*
1070 *Science* **108**, 100616 (2019).
- 1071 155. Smolin, Y. Y., Soroush, M. & Lau, K. K. Influence of oCVD polyaniline film chemistry in carbon-based
1072 supercapacitors. *Industrial & Engineering Chemistry Research* **56**, 6221-6228 (2017).
- 1073 156. Lau, K. K. & Gleason, K. K. Initiated chemical vapor deposition (iCVD) of poly (alkyl acrylates): an
1074 experimental study. *Macromolecules* **39**, 3688-3694 (2006).
- 1075 157. Tao, R. & Anthamatten, M. Condensation and Polymerization of Supersaturated Monomer Vapor.
1076 *Langmuir* **28**, 16580-16587 (2012).
- 1077 158. O'Shaughnessy, W., Murthy, S., Edell, D. & Gleason, K. Stable biopassive insulation synthesized by
1078 initiated chemical vapor deposition of poly (1, 3, 5-trivinyltrimethylcyclotrisiloxane). *Biomacromolecules* **8**,
1079 2564-2570 (2007).
- 1080 159. Obratsov, A. N., Obratsova, E. A., Tyurnina, A. V. & Zolotukhin, A. A. Chemical vapor deposition of
1081 thin graphite films of nanometer thickness. *Carbon* **45**, 2017-2021 (2007).
- 1082 160. Yu, Q. *et al.* Graphene segregated on Ni surfaces and transferred to insulators. *Appl Phys Lett* **93**, 113103
1083 (2008).
- 1084 162. Lee, Y. *et al.* Wafer-Scale Synthesis and Transfer of Graphene Films. *Nano Lett* **10**, 490-493 (2010).
- 1085 163. Hong, B. H. *et al.* Graphene roll-to-roll coating apparatus and graphene roll-to-roll coating method using
1086 the same. United States KR1020100011437 patent (2010).
- 1087 164. Han, T.-H. *et al.* Extremely efficient flexible organic light-emitting diodes with modified graphene anode.
1088 *Nature Photonics* **6**, 105-110 (2012).
- 1089 165. Kang, J. *et al.* High-Performance Graphene-Based Transparent Flexible Heaters. *Nano Lett* **11**, 5154-5158
1090 (2011).
- 1091 166. Kang, S. *et al.* Efficient heat generation in large-area graphene films by electromagnetic wave absorption.
1092 *2D Materials* **4**, 025037 (2017).

- 1093 167. Kobayashi, T. *et al.* Production of a 100-m-long high-quality graphene transparent conductive film by roll-
1094 to-roll chemical vapor deposition and transfer process. *Appl Phys Lett* **102**, 023112 (2013).
- 1095 168. Hesjedal, T. Continuous roll-to-roll growth of graphene films by chemical vapor deposition. *Appl Phys Lett*
1096 **98**, 133106 (2011).
- 1097 169. Zhong, G. *et al.* Growth of continuous graphene by open roll-to-roll chemical vapor deposition. *Appl Phys*
1098 *Lett* **109**, 193103 (2016).
- 1099 170. Polsen, E. S., McNerny, D. Q., Viswanath, B., Pattinson, S. W. & John Hart, A. High-speed roll-to-roll
1100 manufacturing of graphene using a concentric tube CVD reactor. *Sci Rep-Uk* **5**, 10257 (2015).
- 1101 171. Kim, D. J. *e. a.* Confocal laser scanning microscopy as a real time quality-assessment tool for industrial
1102 graphene synthesis. *2D Materials* **7**, 045014 (2020).
- 1103 172. Hong, B. H. Commercial Scale Production of CVD Graphene and Graphene Quantum Dots. *Phantom*
1104 *Foundation*, Graphene Industrial Forum 2020 (2020).
- 1105 173. Robertson, J., Liu, X., Yue, C., Escarra, M. & Wei, J. Wafer-scale synthesis of monolayer and few-layer
1106 MoS₂ via thermal vapor sulfurization. *2D Materials* **4**, 045007 (2017).
- 1107 174. Lim, Y. R. *et al.* Roll-to-Roll Production of Layer-Controlled Molybdenum Disulfide: A Platform for 2D
1108 Semiconductor-Based Industrial Applications. *Advanced Materials* **30**, 1705270 (2018).
- 1109 175. Hempel, M. *et al.* Repeated roll-to-roll transfer of two-dimensional materials by electrochemical
1110 delamination. *Nanoscale* **10**, 5522-5531 (2018).
- 1111 176. Jeon, W., Cho, Y., Jo, S., Ahn, J.-H. & Jeong, S.-J. Wafer-Scale Synthesis of Reliable High-Mobility
1112 Molybdenum Disulfide Thin Films via Inhibitor-Utilizing Atomic Layer Deposition. *Advanced Materials*
1113 **29**, 1703031 (2017).
- 1114 177. Choi, T. *et al.* Roll-to-roll continuous patterning and transfer of graphene via dispersive adhesion.
1115 *Nanoscale* **7**, 7138-7142 (2015).
- 1116 178. Jo, I. *et al.* Tension-controlled single-crystallization of copper foils for roll-to-roll synthesis of high-quality
1117 graphene films. *2D Materials* **5**, 024002 (2018).
- 1118 179. Jin, S. *et al.* Colossal grain growth yields single-crystal metal foils by contact-free annealing. *Science* **362**,
1119 1021 (2018).
- 1120 180. Lee, J. S. *et al.* Wafer-scale single-crystal hexagonal boron nitride film via self-collimated grain formation.
1121 *Science* **362**, 817 (2018).
- 1122 181. Kim, Y.-J., Kim, Y., Novoselov, K. & Hong, B. H. Engineering electrical properties of graphene: chemical
1123 approaches. *2D Materials* **2**, 042001 (2015).
- 1124 182. Zhao, L. *et al.* Visualizing Individual Nitrogen Dopants in Monolayer Graphene. *Science* **333**, 999 (2011).
- 1125 183. Kim, Y. *et al.* Vapor-Phase Molecular Doping of Graphene for High-Performance Transparent Electrodes.
1126 *ACS Nano* **8**, 868-874 (2014).
- 1127 184. Kim, Y. *et al.* A highly conducting graphene film with dual-side molecular n-doping. *Nanoscale* **6**, 9545-
1128 9549 (2014).
- 1129 185. Jo, I. *et al.* Stable n-type doping of graphene via high-molecular-weight ethylene amines. *Physical*
1130 *Chemistry Chemical Physics* **17**, 29492-29495 (2015).
- 1131 186. Yan, C. *et al.* Mechanical and Environmental Stability of Polymer Thin-Film-Coated Graphene. *ACS Nano*
1132 **6**, 2096-2103 (2012).
- 1133 187. Choi, K. *et al.* Reduced Water Vapor Transmission Rate of Graphene Gas Barrier Films for Flexible
1134 Organic Field-Effect Transistors. *ACS Nano* **9**, 5818-5824 (2015).
- 1135 188. Kim, D. J. *et al.* Degradation Protection of Color Dyes Encapsulated by Graphene Barrier Films. *Chemistry*
1136 *of Materials* **31**, 7173-7177 (2019).
- 1137 189. Kim, J. *et al.* Low-temperature synthesis of large-area graphene-based transparent conductive films using
1138 surface wave plasma chemical vapor deposition. *Appl Phys Lett* **98**, 091502 (2011).
- 1139 190. Havener, R. W. *et al.* High-Throughput Graphene Imaging on Arbitrary Substrates with Widefield Raman
1140 Spectroscopy. *ACS Nano* **6**, 373-380 (2012).
- 1141 191. Krupka, J., Strupinski, W. & Kwietniewski, N. Microwave Conductivity of Very Thin Graphene and Metal
1142 Films. *Journal of Nanoscience and Nanotechnology* **11**, 3358-3362 (2011).
- 1143 192. Whelan, P. R. *et al.* Robust mapping of electrical properties of graphene from terahertz time-domain
1144 spectroscopy with timing jitter correction. *Opt. Express* **25**, 2725-2732 (2017).
- 1145 193. Panchal, V. *et al.* Confocal laser scanning microscopy for rapid optical characterization of graphene.
1146 *Communications Physics* **1**, 83 (2018).
- 1147 194. Ci, L. *et al.* Preparation of carbon nanofibers by the floating catalyst method. *Carbon* **38**, 1933-1937 (2000).

- 1148 195. Wang, B. W. *et al.* Continuous Fabrication of Meter-Scale Single-Wall Carbon Nanotube Films and their
1149 Use in Flexible and Transparent Integrated Circuits. *Adv Mater* **30**, e1802057 (2018).
- 1150 196. Huang, J.-K. *et al.* Large-Area Synthesis of Highly Crystalline WSe₂ Monolayers and Device Applications.
1151 *ACS Nano* **8**, 923-930 (2014).
- 1152 197. Geng, D. *et al.* Direct Synthesis of Large-Area 2D Mo₂C on In Situ Grown Graphene. *Adv Mater* **29**
1153 (2017).
- 1154 198. Coclite, A. M. *et al.* 25th anniversary article: CVD polymers: A new paradigm for surface modification
1155 and device fabrication. *Advanced Materials* **25**, 5392-5423 (2013).
- 1156 199. Zhou, H. & Bent, S. F. Fabrication of organic interfacial layers by molecular layer deposition: Present
1157 status and future opportunities. *Journal of Vacuum Science & Technology A: Vacuum, Surfaces, and Films*
1158 **31**, 040801 (2013).
- 1159 200. George, S. M., Yoon, B. & Dameron, A. A. Surface Chemistry for Molecular Layer Deposition of Organic
1160 and Hybrid Organic–Inorganic Polymers. *Accounts of chemical research* **42**, 498-508 (2009).
- 1161 201. Bilger, D., Homayounfar, S. Z. & Andrew, T. L. A critical review of reactive vapor deposition for
1162 conjugated polymer synthesis. *Journal of Materials Chemistry C* **7**, 7159-7174 (2019).
- 1163 202. Gharahcheshmeh, M. H. & Gleason, K. K. Engineering texture and nanostructure in conjugated conducting
1164 and semiconducting polymers. *Materials Today Advances* **8**, 100086 (2020).
- 1165 203. Chen, H.-Y. & Lahann, J. Designable biointerfaces using vapor-based reactive polymers. *Langmuir* **27**, 34-
1166 48 (2011).
- 1167 204. Hassan, Z., Spuling, E., Knoll, D. M. & Bräse, S. Regioselective functionalization of [2.2] paracyclophanes:
1168 Recent synthetic progress and perspectives. *Angewandte Chemie International Edition* **59**, 2156-2170
1169 (2020).
- 1170 205. Yasuda, H. K. & *Plasma polymerization* (Academic Press Inc, New York, 1985).
- 1171 206. Kovacic, P., del Hierro, G., Livernois, W. & Gleason, K. K. Scale-up of oCVD: large-area conductive
1172 polymer thin films for next-generation electronics. *Materials Horizons* **2**, 221-227 (2015).
- 1173 207. Barr, M. C. *et al.* Direct monolithic integration of organic photovoltaic circuits on unmodified paper.
1174 *Advanced Materials* **23**, 3500-3505 (2011).
- 1175 208. Lau, K. K. *et al.* Superhydrophobic carbon nanotube forests. *Nano Lett* **3**, 1701-1705 (2003).
- 1176 209. Yang, S. C. *et al.* Large - Scale, Low - Power Nonvolatile Memory Based on Few - Layer MoS₂ and
1177 Ultrathin Polymer Dielectrics. *Advanced Electronic Materials* **5**, 1800688 (2019).

1178

1179

1181 Highlighted review is missing:

1182 Cai, Z., Liu, B., Zou, X. & Cheng, H. M. Chemical Vapor Deposition Growth and Applications of Two-
1183 Dimensional Materials and Their Heterostructures. Chem Rev 118, 6091-6133 (2018). This is a
1184 systematic introduction to CVD growth of two-dimensional materials and their hetrostructures.

1185

1186 Acknowledgments

1187 Z.F.L. and L.Z.S. were supported by Beijing National Laboratory for Molecular Sciences (BNLMS-
1188 CXTD-202001), Beijing Municipal Science & Technology Commission (No. Z181100004818001,
1189 Z191100000819005), the National Basic Research Program of China (No. 2016YFA0200101) and
1190 the National Natural Science Foundation of China (Nos. 21525310, 51432002, and
1191 51520105003).

1192 Author contributions:

1193 Introduction (Z.F.L and L.Z.S); Experimentation (Z.F.L. and L.Z.S.); Results (L.B.G. and G.W.Y.);
1194 Applications (M.C., J.E.Y., K.K.G., M.H.G., B.H.H., and Y.S.C.); Reproducibility and data deposition
1195 (B.H.H. and Y.S.C.); Outlook (M.C. and J.E.Y.); Overview of Primer (Z.F.L.). All authors discussed
1196 and edited the full manuscript.

1197 Competing interests

1198 K.K.G is a co-founder of GVD Corporation and DropWise Technologies. Both companies are
1199 commercializing CVD polymerization.

1200

1201 Peer review information

1202 *Nature Reviews Methods Primers* thanks Jong-Hyun Ahn , Toshiyuki Kobayashi , Gözde İnce, A.N
1203 Obratsov, Florian Stadler and the other, anonymous, reviewer(s) for their contribution to the
1204 peer review of this work.

1205

1206

1207

Tables

1208

1209

Table 1. Carbon solubility and thermal expansion properties of CVD substrates^{60,61}

Substrates	Carbon solubility at 1000 °C (at.%) ⁶⁰	Coefficient of thermal expansion (10 ⁻⁶ K ⁻¹) ⁶¹
Graphene	-	-7
Cu	0.04	16.7
Ni	1.3	12.8
Pt	1.76	8.9
Co	3.41	13.7
Ru	1.56	6.7
Pd	5.98	11.6
Ir	1.35	6.5
SiC	-	3.5
Si	-	2.5
Quartz (SiO ₂)	-	0.4
Sapphire (Al ₂ O ₃)	-	5.0–5.6

1210

1211

1212

1213

1214

Table 2. Characterization tools and their settings for assessing graphene quality and structure.

Assessment tool(s)	Spatial resolution	Property	Advantages	Disadvantages	Considerations
Optical microscopy	$\leq \mu\text{m}$	individual domain shapes; surface coverage; number of layers ; grain boundaries; defects (wrinkles and folds)	Simple to operate; Large-area characterization; non-destructive to the sample	low resolution; usually needs a suitable substrate	Clearer images when choosing a suitable wavelength of light or adding an optical filter
scanning electron microscopy	$\sim \text{nm}$	individual domain shapes; surface coverage; number of layers ; grain boundaries; Defects (wrinkles and folds)	Simple to operate; Large-area characterization; High-resolution; Good environmental adaptability	damages the graphene atomic lattice	Based on electron scattering; the electron beam energy ranges from a few 100 eV to a few keV
atomic force microscopy	$\leq \text{nm}$	individual domain shapes; surface coverage; roughness; grain boundaries; number of layers	High-resolution; Good environmental adaptability	Scanned area is small; scanning speed is slow; unsuitable for samples with significant surface topography	Sample surface must be clean. Pollutants contaminate the tip and can result in virtual and/or false images.
scanning tunneling microscopy	$\leq \text{\AA}$	Atomic structures (e.g. point defects, grain boundaries); crystal orientation	Atomic resolution; non-destructive	scanned area is small; substrate must be conductive and ultra-smooth; complex and expensive	Based on quantum tunneling effect; two possible operation modes (constant current or constant height)

transmission electron microscopy	$\leq \text{\AA}$	Atomic structures (e.g. point defects, grain boundaries); crystal orientation; purity	Atomic resolution; can obtain cross-section geometry	as-grown graphene must be transferred to a suitable substrate	high energy electron beam (several 10 keV to few 100 keV) can induce defects
Raman spectroscopy	$\sim 100 \text{ nm}$ (diffraction limit)	number of layers; defects; strain; doping	simple to operate; High sensitivity Spatially-resolved distribution can be easily obtained by mapping the sample	qualitative only	SiO_2 is the most frequently used substrate
X-ray photoelectron spectroscopy	$100 \mu\text{m}$	purity	Surface sensitive technique to analyze elemental composition and chemical state	Low spatial resolution; no accurate quantification	Detecting depth ranges from 1 nm to 10 nm
angular resolution photoemission spectroscopy	$\sim \text{meV}$ (relies on the resolution of the analyzer, the sample and the UV source)	Electronic properties (band structure); doping	band structure can be directly observed; as-grown graphene can be directly characterized	The band structure above the Fermi surface cannot be obtained; complex and expensive	Based on the photoelectric effect

1215

1216

Table 3. Summary of typical CVD methods for growing 2D materials

Materials	Substrate	Precursor 1	Precursor 2	Key parameters	Remarks	References
<i>h</i> BN	Cu, Ni, Pt, SiO ₂ , Sapphire	NH ₃ -BH ₃ (heating at 60 ~100 °C)	-	LPCVD with H ₂ /Ar flow, at ~1000°C	Single crystal substrate with steps can induce the mono-orientation of <i>h</i> BN	98,129,130
MS ₂ (M=Mo, W, etc.)	SiO ₂ , Mica	S powder (heating at 100 ~ 200 °C)	MO ₃ (near the hot center)	APCVD or LPCVD, with H ₂ /Ar flow at 600 ~ 900 °C	NaCl or KCl can serve as promoters for improving the quality and growth rate of these 2D TMDs.	17,127,129
		(C ₂ H ₅) ₂ S (0.4 sccm)		MOCVD, at ~1000 Pa, 550 °C		124
MSe ₂ (M=Mo, W, etc.)		Se powder (heating at 200 ~ 300 °C)	MO ₃ (near the hot center)	APCVD or LPCVD, with H ₂ /Ar flow, at 750 °C ~850 °C		116,127,196
Mo ₂ C, TaC	Mo, Ta	CH ₄ , C ₂ H ₂	-	APCVD, at ~1100 °C	Molten copper plays an important role in the catalytic growth process	131,132,197
Bi ₂ O ₂ Se	Mica, SrTiO ₃	Bi ₂ Se ₃ (Heating at 650~700 °C)	Bi ₂ O ₃ (Heating at 650~700 °C)	LPCVD, with Ar/O ₂ flow at 500 ~600 °C	Substrate with quadruple symmetry (SrTiO ₃) is important for epitaxial growth of single-crystal Bi ₂ O ₂ Se	19,134

1217

1218 **Table 4. Summary of CVD polymer growth methods.** Typical reactants, solution-phase analogy,
1219 and polymer backbone structure for different CVD polymerization methods

1220

CVD polymerization method	Typical Reactants	Analogous Solution	Structure of Polymer	References
---------------------------	-------------------	--------------------	----------------------	------------

		Mechanism	Backbone	
initiated CVD (iCVD)	initiator + monomer(s)	chain growth	carbon single bonds	142,198
molecular layer deposition (MLD)	pair of monomers	condensation	includes heteroatoms (e.g. O,N)	199,200
oxidative CVD (oCVD)	oxidant + monomer(s)	step growth	alternating single and double bonds	152,201,202
poly(p-xylylenes) (parylene)	dimer	none	hydrocarbon	203,204
plasma enhanced CVD (PECVD)	volatile precursor(s)	none	various, typically crosslinked	205

1221

1222

Figure legends

1223
1224

1225 **FIG. 1 | Schematic diagram of general elementary steps of typical CVD process.** First, reactant gases
1226 (blue circles) are transported into the reactor (a). Then, there are two possible routes for the reactant
1227 gases: directly diffusing through the boundary layer (b) and adsorbing onto the substrate (c); forming
1228 intermediate reactants (green circles) and by products (red circles) via the gas-phase reaction (d) and
1229 deposited onto the substrate by diffusion (b) and adsorption (c). Surface diffusion and heterogeneous
1230 reactions (e) take place on the surface of substrate before the formation of thin films or coatings. Finally,
1231 by-products and unreacted species are desorbed from the surface and forced out of the reactor as
1232 exhausts (f).

1233

1234 **FIG. 2 | Typical CVD equipment.** **a.** Schematic diagram of a typical horizontal CVD system, which
1235 includes: a gas delivery system, the quartz reaction chamber, a vacuum system, the energy system and
1236 an auto-control system. **b.** A photograph of liquid precursor bubbler, which can also be used to provide
1237 solid precursors by dissolution in a suitable solvent. **c -f.** A vertical reactor for scalable growth of
1238 graphene wafers, where the 25 wafers can be loaded on the quartz substrate holder (**c**). The multiple
1239 gas inlet nozzles are designed (**d**) to improve the uniformity of gas flow, which is simulated based on
1240 finite element method (**e**)²⁵. Bourdon gauge (**f**) and capacitance manometer (**g**), which are commonly
1241 used to measure the pressure of the vacuum system. Parts d-f adapted with permission from ref 25,
1242 Elsevier.

1243

1244 **FIG. 3 | Schematic of experimental process for growing graphene.** **a-d**, the processes of growing
1245 graphene on metal substrates: (**a**) electrochemical polishing for cleaning and smooth the substrate, (**b**)

1246 heating and annealing to reduce the nucleation sites and enlarge the grain size of metal substrate, (c)
1247 high-temperature growth which is dominated by the surface reaction, (d) (d) Precipitation and
1248 crumpling during the cooling process. e-g, the processes of growing graphene on dielectric substrates: (e)
1249 Cleaning the dielectric substrate, (f) gas-phase reaction dominated growth at high-temperature, (g)
1250 thermal contraction induced crumpling during the cooling process.

1251

1252 **FIG.4 | Characterization of CVD-grown graphene.** a. Optical microscopy image of the transferred film
1253 on SiO₂/Si substrate, the layer number can be distinguished by the color contrast⁶⁶. Scale bar 50 μm. b.
1254 SEM image of graphene domains grown on platinum foil, copper surface roughing changes with the
1255 number of graphene layers⁶⁷. Scale bar 1 mm. c. Typical AFM image of graphene grown on copper foil⁷⁸.
1256 Scale bar 2 μm. d. AFM image of graphene grown on Cu(111), where there are some wrinkles and folds⁹⁰.
1257 Scale bar 1 μm. e. STM image (sample bias -2V, tunnelling current 50 pA) near a corner of a hexagonal
1258 graphene grain on copper foil. Scale bar 1 μm. f. Atomic-resolution STM image corresponding to the
1259 green frame in (e)⁸⁰. Scale bar 3.2 Å. g. Graphene-hBN boundary structure imaged by atomic-resolution
1260 STM⁸⁹. Scale bar 1 nm. h. Atomic-resolution TEM image of the typical grain boundary in CVD-grown
1261 graphene film⁹⁴. Scale bar 0.5 nm. i. Typical Raman spectra of CVD graphene on copper⁷⁸. j. Raman
1262 spectra of monolayer, AB-stacked bilayer and ABA-stacked tri-layer graphene transferred onto SiO₂/Si
1263 substrates⁶⁶. k. Typical ARPES of the as-grown monolayer graphene on Cu(111)⁹⁰. l. STS spectra of the
1264 graphene films on Cu(111)⁹⁰. ARPES, Angle-resolved photoemission spectroscopy; STM, scanning
1265 tunneling microscopy; STS, scanning tunneling spectroscopy. Parts a, j reprinted from ref. 66, Springer
1266 Nature Limited. Part b reprinted from ref.67, Springer Nature Limited. Parts c, i adapted with permission
1267 from ref 78, American Chemical Society. Parts d, k-l adapted from ref.90, Springer Nature Limited. Parts

1268 e-f reprinted from ref.80, Springer Nature Limited. Part g reprinted with permission from ref 89, AAAS.

1269 Part 4h reprinted from ref.94, Springer Nature Limited.

1270

1271 FIG. 5 | Schematic of the typical components of a tube furnace used to grow MoS₂ and similar TMDs.

1272 Typical reaction pathway for MoS₂ by thermal CVD is: $\text{MoO}_3(\text{s}) + \frac{x}{2}\text{S}(\text{g}) \xrightarrow{650^\circ\text{C}} \text{MoO}_{3-x}(\text{g}) + \frac{x}{2}\text{SO}_2$;

1273 Bulk transport of MoO_{3-x} (g) and S (g); Surface adsorption of MoO_{3-x} (g) and S (g); MoO_{3-x} +

1274 $(3 - \frac{x}{2})\text{S} \xrightarrow{800^\circ\text{C}} \text{MoOS}_2 + (1 - \frac{x}{2})\text{SO}_2$; $\text{MoOS}_2 \xrightarrow{800^\circ\text{C}} \text{MoS}_2(\text{s}) + \frac{1}{2}\text{O}_2(\text{g})$; Bulk transport of O₂

1275 away from the chamber. An optical microscopy image of typical triangular single crystal MoS₂

1276 monolayers is also shown¹²⁹. Adapted with permission from ref 129, American Chemical Society.

1277

1278 **FIG. 6| Selected examples of CVD polymer processing and applications. a.** Roll-to-roll vacuum chamber,

1279 300 mm wide, for CVD polymerization²⁰⁶. **b.** An foldable solar cell, ~ 2 cm x 2 cm, fabricated directly on

1280 top of ordinary paper as the substrate, enabled by the low temperature deposition and patterning of a

1281 CVD transparent conducting polymer²⁰⁷. **c.** Dual-scale pattern in silicon, including sub-10 nm lines and

1282 spaces, created using a CVD polymerization¹⁴⁷. **d.** Flexible and conformal CVD polymer encapsulation of

1283 a 25 μm diameter lead wire for a biomedical implant¹⁵⁸. **e.** A nearly spherical water drop on a

1284 superhydrophobic surface created by a CVD fluoropolymer grown conformally over a nanostructured

1285 array²⁰⁸. **f.** Ultrathin CVD polymer dielectric (pV3D3) for low-power flash memory²⁰⁹. (A) Reproduced

1286 with permission²⁰⁶. Copyright 2015, Royal Society of Chemistry. (B) Reproduced with permission²⁰⁷.

1287 Copyright 2012, Wiley. (C) Reproduced with permission¹⁴⁷. Copyright 2017, Nature. (D) Reproduced with

1288 permission¹⁵⁸. Copyright 2007, American Chemical Society. (E) Reproduced with permission²⁰⁸. Copyright

1289 2003, American Chemical Society. (F) Reproduced with permission²⁰⁹. Copyright 2019, Wiley. Part a

1290 adapted with permission from Ref 206, The Royal Society of Chemistry. Part b adapted with permission
1291 from Ref 207, Wiley. Part c adapted from ref.147, Springer Nature Limited. Part d adapted with
1292 permission from Ref 158, American Chemical Society. Part e adapted with permission from ref 208,
1293 American Chemical Society. Part f adapted with permission from ref 209, Wiley.

1294

1295 **FIG. 7 | Advances in CVD technology for scaling-up graphene synthesis.** a, A timeline highlighting the
1296 advances in CVD technology to scale-up graphene synthesis from a manual 2-inch (5 cm) thermal CVD
1297 furnace to a fully automated 50 cm wide R2R system. b Post-CVD processes that utilize the R2R method
1298 for the continuous production of graphene films, including etching and laminated transfer of CVD
1299 graphene films to target substrates (Ref.⁷⁹). Part b, image courtesy of Yong Seok Choi, Graphene Square
1300 Inc. Part c adapted from ref.79, Springer Nature Limited.

1301

1302 **FIG. 8 | The full roll-to-roll (R2R) production of graphene films.** Starting with the R2R CVD synthesis of
1303 graphene on copper (yellow), R2R lamination, R2R etching/doping, and R2R patterning/transfer to
1304 target substrates (blue) for graphene film production. Figure 8 is reprinted from ref 171, CC BY 4.0
1305 (<https://creativecommons.org/licenses/by/4.0/>).

1306

1307 **FIG. 9 | Important factors that determine the reliability of graphene synthesis, and the corresponding**
1308 **electrical performance data.** a. Illustration on the multi-zone heaters with graphite susceptors. b.
1309 Reproducibility of sheet resistance for 10 different growth trials. c, Spatial sheet resistance distribution
1310 of the graphene films. d. Time-durability of the graphene films monitored at 85 °C with 85% humidity for
1311 12 weeks. Inset: resistivity of the graphene synthesized by rapid thermal CVD as a function of back gate

1312 voltage (V_{bg}) at room temperature, which indicates the carrier mobility is as high as $5290 \text{ cm}^2 \text{ V}^{-1} \text{ s}^{-1}$.
1313 Parts a-d adapted with permission from ref 36, American Chemical Society.

1314

1315 **FIG. 10 | Concept of *in-situ* monitoring of the as-grown CVD graphene on Cu using CLSM.** a. The
1316 concept of monitoring the as-grown CVD graphene on Cu foil during the continuous roll-to-roll synthetic
1317 process using the reflective mode CLSM. **b-d**, The CLSM images of the CVD graphene grown for 10, 13,
1318 and 30 min, respectively. Scale bar: $10\mu\text{m}$. Figure 10a-d is reprinted from ref 171, CC BY 4.0
1319 (<https://creativecommons.org/licenses/by/4.0/>).

1320

1321 Box

1322

1323 [bH1] BOX 1 | CVD categories and variants

1324 [bH2] **Horizontal CVD and vertical CVD** are based on the reactor configurations or the directions of gas
1325 flow. The horizontal tube reactor is the most common configuration, where the substrates are mounted
1326 horizontally, vertically, or with a tilt angle, to adjust the gas flow. The vertical reactor is usually equipped
1327 with a showerhead mixer, which is beneficial for material uniformity and growth rate.

1328 [bH2] **Low pressure CVD (LPCVD) and atmospheric pressure CVD (APCVD)** are based on the working
1329 pressure. In LPCVD, a vacuum pump drives the gas flow. In contrast, APCVD usually does not require a
1330 pump and results in a slow flow rate for the reactive gas.

1331 [bH2] **Hot-wall CVD and cold-wall CVD** refer to the heating methods of thermal CVD. In hot-wall CVD,
1332 the entire reaction chamber is heated by an external furnace with a uniform temperature. In cold-wall
1333 CVD, only the substrate and its vicinity are heated, and the reactor wall is cold, allowing for rapid
1334 heating and cooling. Resistance heating, hot plates, and induction heating methods are common for
1335 cold-wall CVD..

1336 **[bH2] Plasma-enhanced CVD (PECVD), and photo-assisted CVD and laser-assisted CVD** are variants of
1337 thermal CVD involving additional components and the introduction of other types of energy to promote
1338 the CVD reaction. In PECVD, plasma, a partially ionized high energy gas, is generated by direct current,
1339 radio frequency voltage, or microwave sources and coupled to the reactor, resulting in a major drop the
1340 reaction temperature. In photo-/laser-assisted CVD, light from a high-intensity lamp or laser is used to
1341 promote the deposition.

1342 **[bH2] Metal-organic CVD (MOCVD)** utilizes metal-organic precursors (usually volatile toxic liquids) that
1343 are vaporized to form thin films. It is widely used to synthesize III-V compound semiconductors (made of
1344 elements from groups III and V in the periodic table) for optoelectronics.

1345 **[bH2] Hot filament/wire CVD (HFCVD/HWCVD)** Resistively-heated filaments (wires) are suspended
1346 above a substrate held at a lower temperature. The filaments cause the thermal decomposition, leading
1347 to precursors, which then adsorb onto the cooler substrates. A refractory metal such as tungsten,
1348 tantalum, or molybdenum, is commonly used as filament material. Typically, inorganic films such as
1349 amorphous silicon or silicon nitride are deposited.

1350 **[bH2] Initiated CVD (iCVD)** is a form of HFCVD/HWCVD for growing electrically insulating polymer thin
1351 films. The iCVD method utilizes an initiator and monomers as vapor-phase reactants, which absorb and
1352 undergo chain-growth polymerization on the cooled substrate. The use of the initiator enables much
1353 lower filament temperatures, which preserves the organic functional groups of the monomer.
1354 Incorporating the functional groups allows control over the wettability and surface reactivity.

1355 **[bH2] oxidative CVD (oCVD)** utilizes oxidant and monomer vapours, which undergo spontaneous
1356 reaction upon adsorption to the substrate. The oCVD produces step-growth polymerization and typically
1357 results in conducting and semiconducting polymer films.

1358 **[bH2] Atomic layer deposition (ALD) and molecular layer deposition (MLD)** are two similar variants of
1359 CVD for depositing inorganic and organic thin films, respectively. For ALD and MLD processes, precursors
1360 are introduced sequentially. Self-limiting absorption and surface reactions of the precursors results in
1361 layer-by-layer growth of high-quality thin films. Between layers the remaining precursor is purged out by
1362 the carrier gas.

1363
1364
1365
1366
1367
1368
1369
1370
1371
1372
1373
1374

1375
1376
1377
1378

1379

1380

1381

1382

1383

1384

1385

1386

1387

1388

1389

1390

1391

1392

1393

1394

1395

Glossary terms

1. Domain: a region of a single crystal, which is delineated by grain boundaries or the edges of an isolated island.
2. Raman scattering: an inelastic scattering of photons by matter, by which the energy of incident photon is changed.
3. Delamination: a phenomenon where layered composites, thin films or coatings separate from the adjacent layers or the substrate due to the weakening of the bonds holding the layers together.
4. half integer Quantum Hall effect: a novel Hall effect quantized into half integer, owing to the peculiar nature of the Landau levels spectrum with energy spacing in graphene, where the Hall conductivity can be described as $\sigma_{xy} = 4e^2/h \left(N + \frac{1}{2}\right)$ (h is Planck constant and $N=0, 1, 2\dots$).

ToC blurb

This Primer on chemical vapour deposition summarizes current and emerging experimental setups as well as common characterisation approaches used to determine thin film formation and quality as applied to graphene and other novel 2D materials.

1396
1397
1398
1399
1400
1401
1402
1403
1404
1405
1406
1407
1408
1409
1410
1411
1412
1413
1414
1415
1416
1417
1418
1419
1420
1421
1422
1423
1424

Handover sheet

Article metadata

1425

1426

1427

1428

Journal, author name, article type:	NRMP, Liu, Primer
Copyright holder (please select):	Springer Nature Limited
Online only	
Sensitive images	[FIGS S,Y,Z]
For MPS (e.g. references that need to be renumbered)	
<p>Duplicate references:</p> <p>Refs 23 and 24 (Deng, B. et al. Roll-to-Roll Encapsulation of Metal Nanowires between Graphene and Plastic Substrate for High-Performance Flexible Transparent Electrodes. Nano Lett 15, 4206-4213 (2015).). I deleted Ref 24. Please convert all instances of reference 24 (duplication of 23) to 23 and renumber the references and the reference list accordingly. Note that reference 24 has been deleted from the reference list.</p> <p>Refs 39 and 161 (Reina, A. et al. Large Area, Few-Layer Graphene Films on Arbitrary Substrates by Chemical Vapor Deposition. Nano Lett 9, 30-35 (2009)). I deleted Ref 161. Please convert all instances of reference 161 (duplication of 39) to 39 and renumber the references and the reference list accordingly. Note that reference 161 has been deleted from the reference list.</p> <p>Refs 65 and 68 (Kim, K. S. et al. Large-scale pattern growth of graphene films for stretchable transparent electrodes. Nature 457, 706-710 (2009).). I deleted Ref 68. Please convert all instances of reference 68 (duplication of 65) to 65 and renumber the references and the reference list accordingly. Note that reference 68 has been deleted from the reference list.</p> <p>Refs 98 and 99 (Chen, T. A. et al. Wafer-scale single-crystal hexagonal boron nitride monolayers on Cu (111). Nature 579, 219-223 (2020).) I deleted Ref 99. Please convert all instances of reference 99 (duplication of 98) to 98 and renumber the references and the reference list accordingly. Note that reference 99 has been deleted from the reference list.</p> <p>Out of order references:</p> <p>Line 271: Ref 68 cited before ref 64-67 (64 is cited line 276).</p> <p>Line 429: Ref 131 cited before refs 126-130.</p> <p>A 'highlighted reference' is missing:</p> <p>Cai, Z., Liu, B., Zou, X. & Cheng, H. M. Chemical Vapor Deposition Growth and Applications of Two-Dimensional Materials and Their Heterostructures. Chem Rev 118, 6091-6133 (2018). This is a systematic introduction to CVD growth of two-dimensional materials and their hetrostructures.</p> <p>Figures are cited in order, but once cited the figure panels are not cited in order. I hope that's OK.</p>	
For PEs (e.g. COVID-19 content, alternative author email address or author availability)	
For copy editing	

1429

1430

1431

1432

1433

1434

1435

1436

1437

1438

1439

1440

1441

1442

1443

1444

1445

Author notes

Please check these figures carefully and return any comments/amendments that you might have to me as soon as possible. In particular, we would like you to check the following:

- Do the figures convey the intended message?
- Are all the labels accurate and in the right place?
- Are all the arrows in the right place?
- Are any chemical structures correct?
- Have shapes and colours been used consistently and accurately throughout the figures?
- Have any of the figures been previously published, or have they been supplied by a colleague(s) who is not a named author on the article?
- For any maps, some style modifications may have been made, are they still correct?

To mark up any corrections, please use the commenting tools in the PDF, or print and draw by hand, rather than directly editing the PDFs.

Fig 1

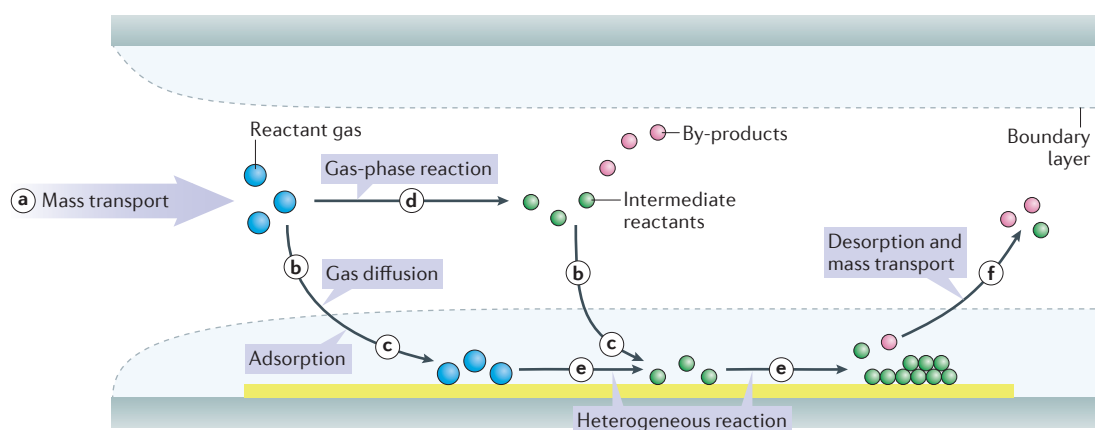


Fig 2

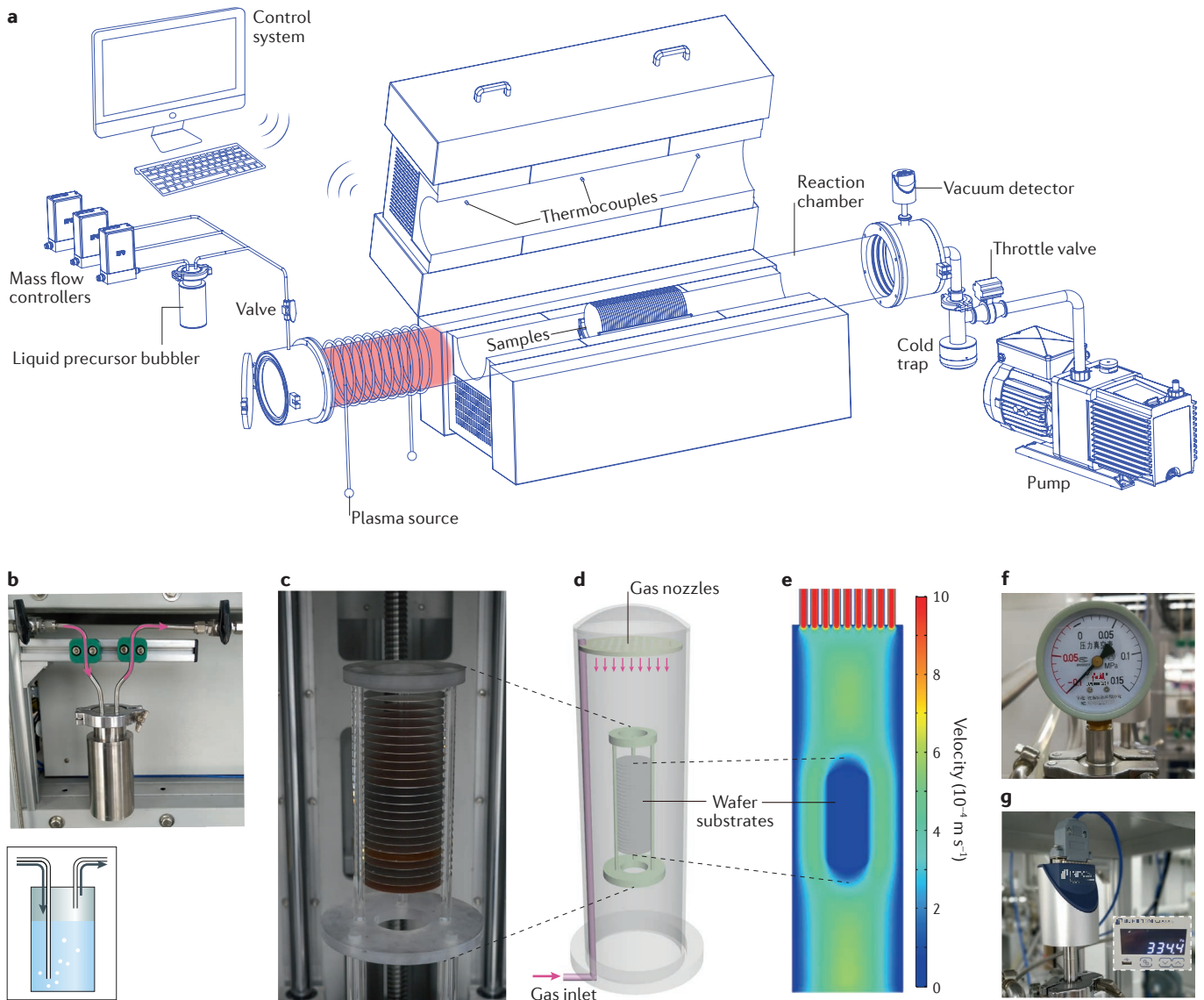


Fig 3

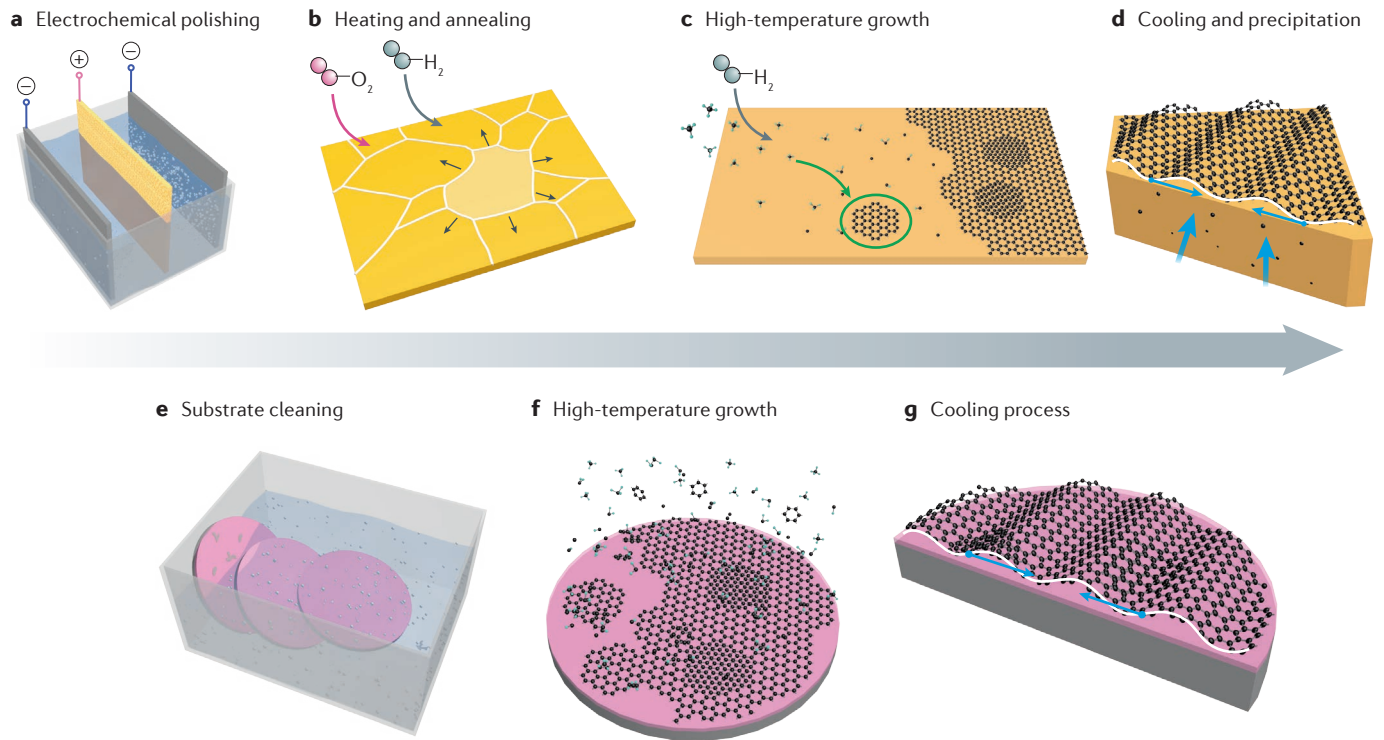


Fig 4

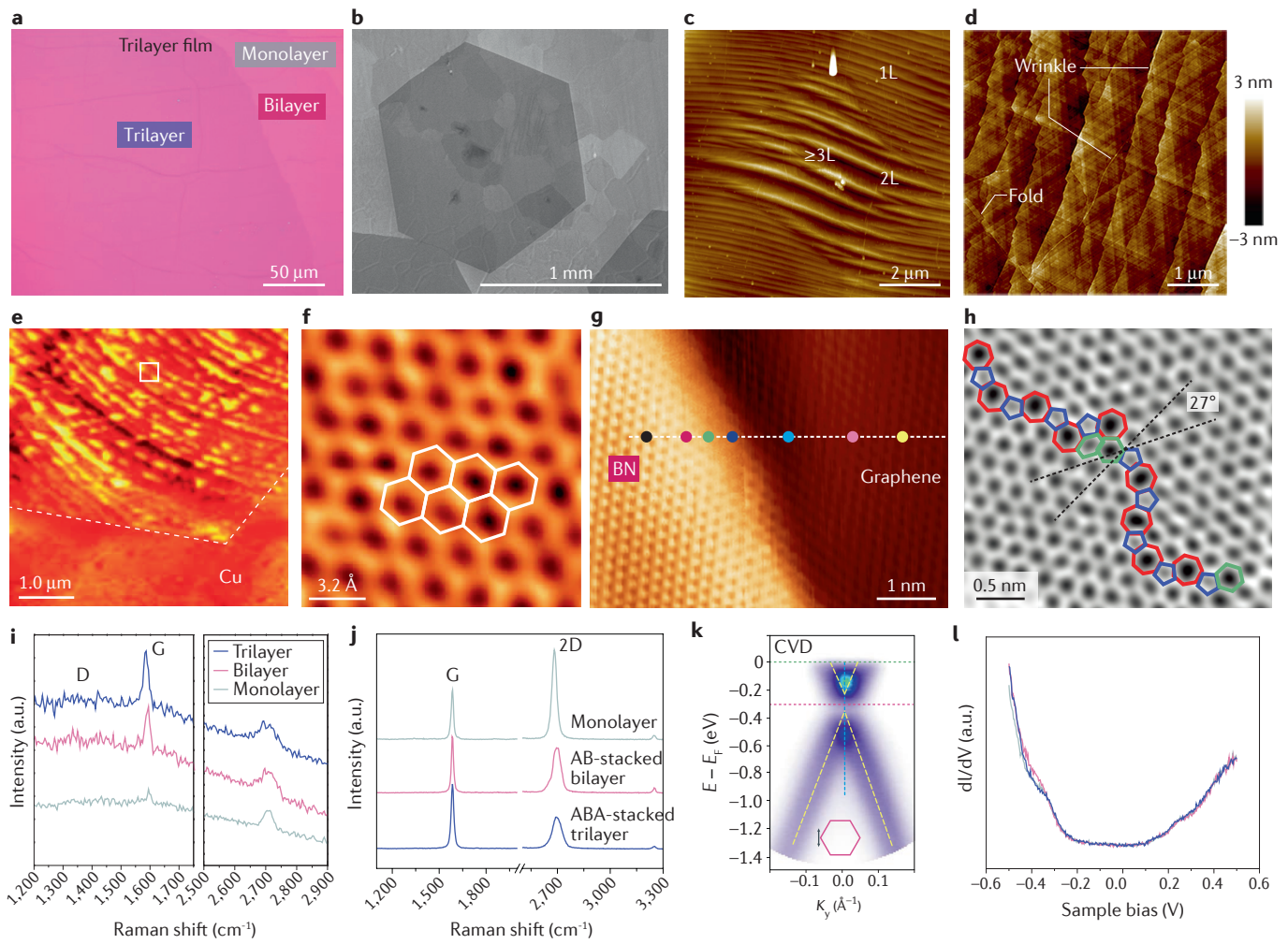


Fig 5

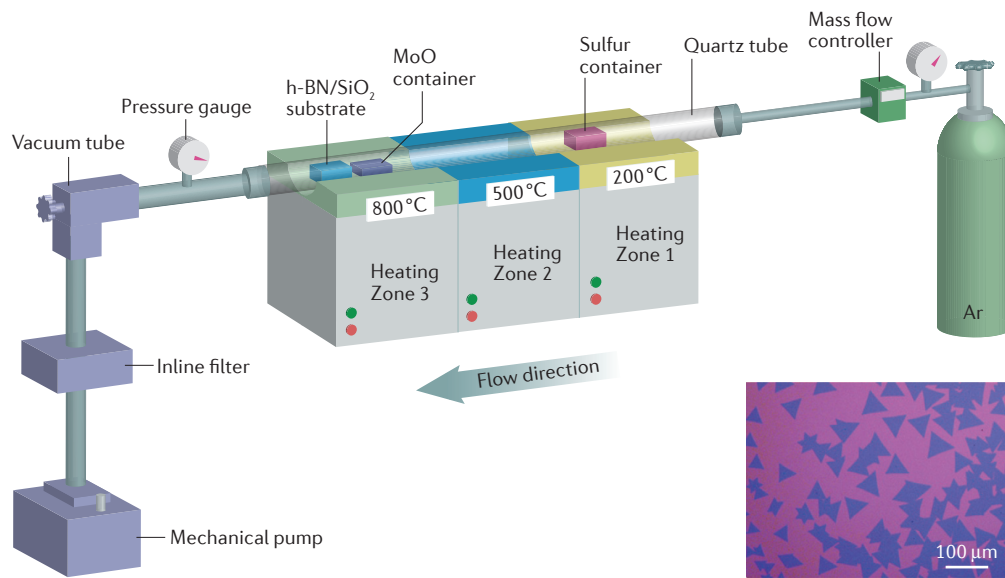


Fig 6

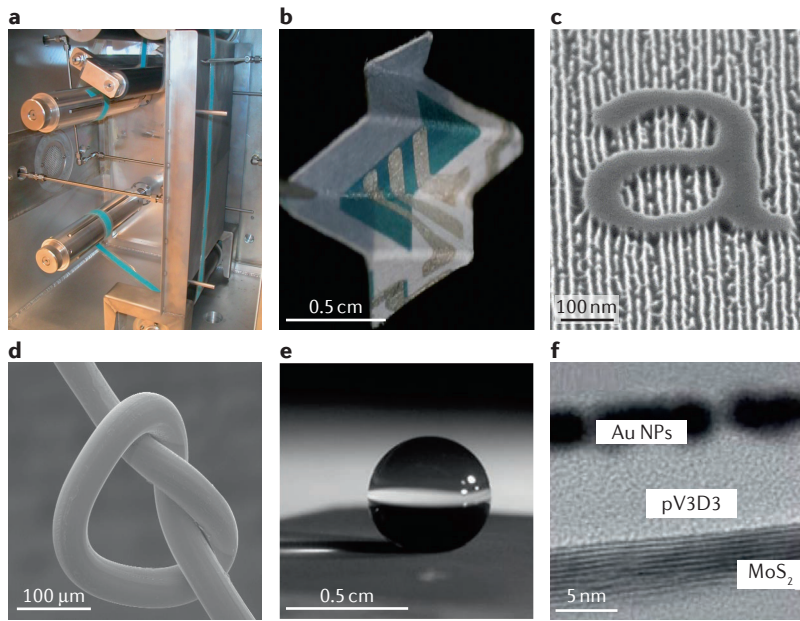


Fig 7

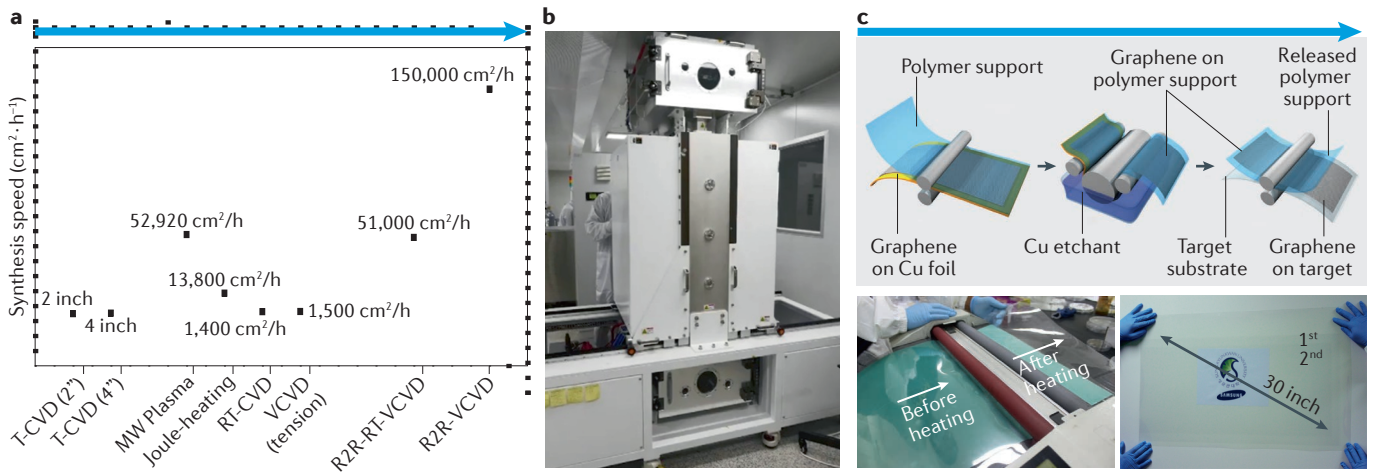


Fig 8

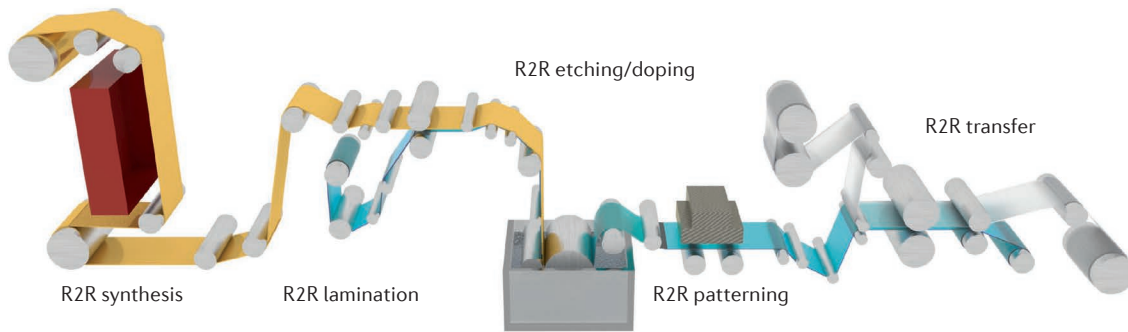


Fig 9

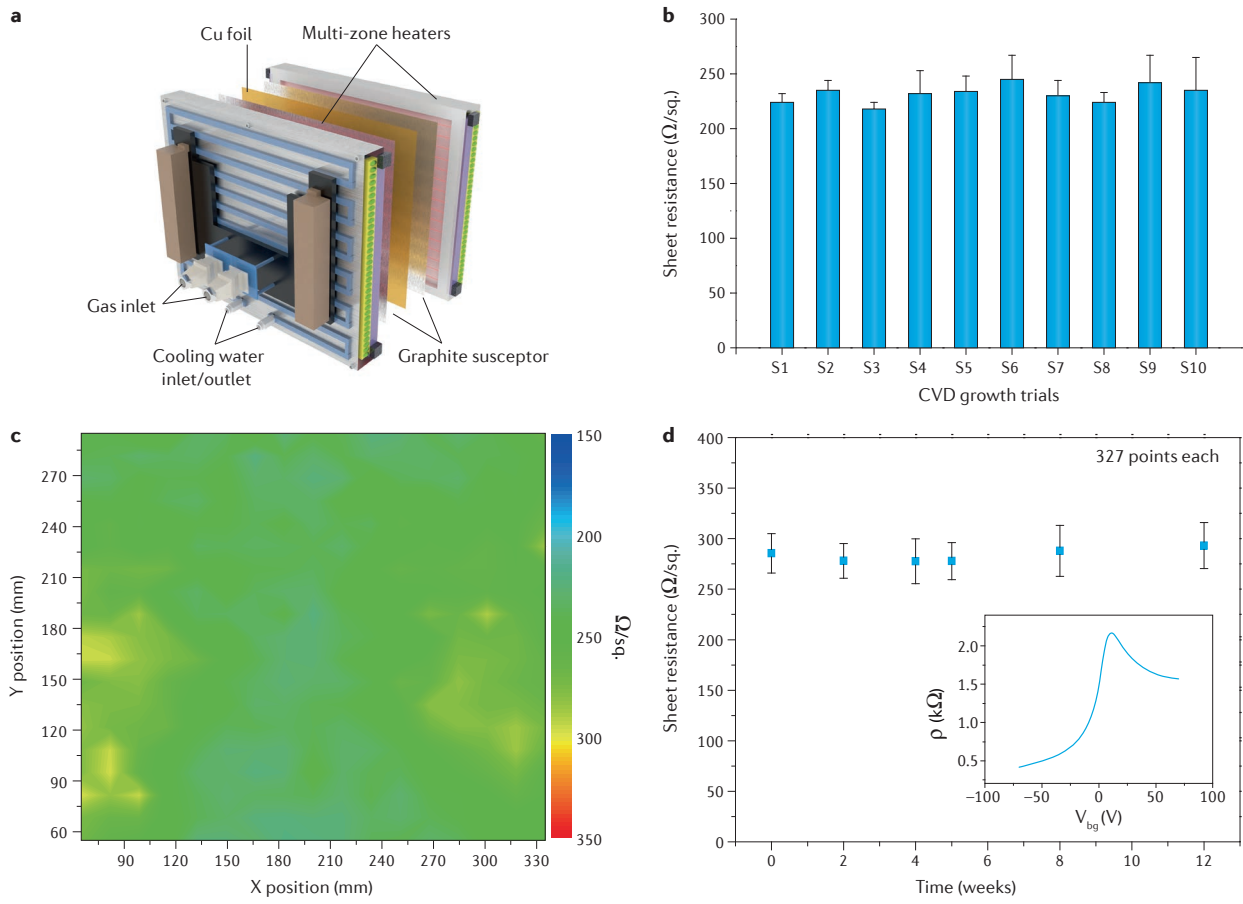


Fig 10

